

Journal Pre-proof



Rational Design of *2H*-chromene-based Antiphytovirals that Inhibit Virion Assembly by Out-Competing Virus Capsid-RNA Interactions

Xiong Yang, Deguo Liu, Chunle Wei, Jianzhuan Li, Chunni Zhao, Yanping Tian, Xiangdong Li, Baoan Song, Runjiang Song

PII: S2589-0042(24)02435-0

DOI: <https://doi.org/10.1016/j.isci.2024.111210>

Reference: ISCI 111210

To appear in: *ISCIENCE*

Received Date: 17 July 2024

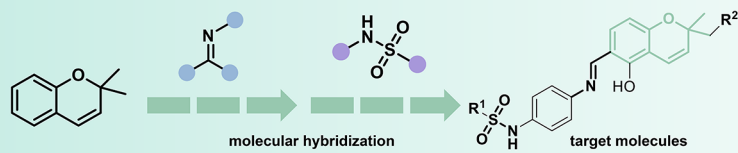
Revised Date: 30 August 2024

Accepted Date: 16 October 2024

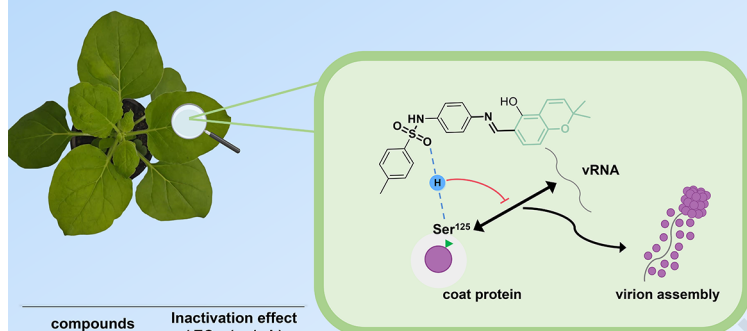
Please cite this article as: Yang, X., Liu, D., Wei, C., Li, J., Zhao, C., Tian, Y., Li, X., Song, B., Song, R., Rational Design of *2H*-chromene-based Antiphytovirals that Inhibit Virion Assembly by Out-Competing Virus Capsid-RNA Interactions, *ISCIENCE* (2024), doi: <https://doi.org/10.1016/j.isci.2024.111210>.

This is a PDF file of an article that has undergone enhancements after acceptance, such as the addition of a cover page and metadata, and formatting for readability, but it is not yet the definitive version of record. This version will undergo additional copyediting, typesetting and review before it is published in its final form, but we are providing this version to give early visibility of the article. Please note that, during the production process, errors may be discovered which could affect the content, and all legal disclaimers that apply to the journal pertain.

© 2024 The Author(s). Published by Elsevier Inc.

Rational design of Novel 2*H*-chromene-based derivatives incorporating sulfonamides and Schiff bases

Discovery and mechanism of action of highly active antiviral C50



compounds	Inactivation effect / EC ₅₀ (μg/mL)
C50	53.3 ± 4.3
Ningnanmycin	75.7 ± 4.0

C50 stops virion assembly by out-competing virus capsid-vRNA interactions at the molecular level

1 **Rational Design of 2*H*-chromene-based Antiphytovirals that Inhibit Virion**
2 **Assembly by Out-Competing Virus Capsid-RNA Interactions**

3 Xiong Yang^{#1}, Deguo Liu^{#2}, Chunle Wei¹, Jianzhan Li¹, Chunni Zhao¹, Yanping Tian^{*2}, Xiangdong
4 Li², Baoan Song¹, Runjiang Song^{*1,3}

5
6 ¹ National Key Laboratory of Green Pesticide, Key Laboratory of Green Pesticide and Agricultural
7 Bioengineering, Ministry of Education, Center for R & D of Fine Chemicals of Guizhou University,
8 Guiyang City, Guizhou province, 550025, P. R. China

9 ² College of Plant Protection, Shandong Agricultural University, Tai'an City, Shandong province,
10 271018, P. R. China

11 [#] Xiong Yang and Deguo Liu contributed equally to this work

12 ^{*} Prof. Runjiang Song and Prof. Yanping Tian are both corresponding authors of this paper

13
14 Corresponding Author:

15 Runjiang Song: songrj@gzu.edu.cn, Yanping Tian: Yanping.tian@sdau.edu.cn

16
17 ³ Lead contact:

18 Runjiang Song (songrj@gzu.edu.cn)

19
20 **SUMMARY**

21 Although the determination of the structural basis of potato virus Y (PVY) coat protein (CP)
22 provides the possibility for CP-based antiviral drug design, the role of many specific residues on CP
23 in regulating virion pathogenicity is largely unknown, and fewer small-molecular drugs have been
24 discovered to act on these potential sites. In this study, a series of derivatives of 2,2-dimethyl-2*H*-
25 chromene are rationally designed by employing a molecular hybridization strategy. We screen a case
26 of phytovirucide **C50** that could form a stable H-bond with Ser¹²⁵ of PVY CP to exert antiviral
27 properties. Ser¹²⁵ is further identified to be crucial for CP-vRNA interaction, enabling PVY virion
28 assembly. This interaction can be significantly inhibited through competitive binding with
29 compound **C50**. The study enhances our understanding of anti-PVY drug mechanisms and provides
30 a basis for developing new CP-targeting virus particle assembly inhibitors.

31

32 INTRODUCTION

33 Potato (*Solanum tuberosum* L.) is one of the crucial essential staple foods on which humanity
34 relies for survival. More than 150 countries and regions worldwide cultivate potato, which serves
35 food, vegetable, and feed functions and has excellent potential for further processing, playing an
36 essential role in ensuring food security¹⁻³. However, plant pests and diseases can lead to crop failure,
37 seriously restricting agricultural production⁴⁻⁶. A notable instance of damaging pests encompasses
38 Potato Virus Y (PVY), a linear RNA-based pathogen categorized within the *Potyviridae* family.
39 Since it was initially reported in 1931, PVY had caused significant damage to crop yields by
40 infecting various cash crops from the *Solanaceae* family, tobacco (*Nicotiana tabacum* L.) and potato
41 being a prominent example.⁷⁻⁹ Currently, managing such viral pests by agrochemicals serves as the
42 most direct route, but there were yet satisfactory results from the exploration of commercial drugs
43 like Ningnanmycin (NNM), ribavirin, and moroxydine for the control of PVY-induced disease
44 (**Figure 1A**), which in turn sparked considerable interest in the development of new molecular
45 entities for PVY management¹⁰⁻¹².

46 The coat protein (CP) plays multiple roles in the PVY life cycle, including virus particle
47 assembly, virus movement, and aphid transmission, etc.¹³. Consequently, CP is considered a
48 promising candidate for biochemical targeting in developing new pesticides with antiviral properties
49 that bind to CP, thereby suppressing virus infection¹⁴. Indeed, CP has emerged as an ideal drug
50 target and has been widely utilized in developing antiviral agents against plant viruses. Many CP
51 inhibitors with diverse chemical structures and activities against various plant viruses have been
52 reported (**Figure 1B**)¹⁵⁻¹⁸. Despite identifying critical sites on the CP that significantly mediate
53 viral pathogenicity, a deeper understanding of molecular interactions remains lacking. Recently, we
54 confirmed that chiral arylimidazole-fused compound **A** could competitively bind to the R¹⁹¹ site of
55 PVY CP, interfering with the mutual effect between CP and the host factor ntCPIP at the molecular
56 level, thereby preventing virions from moving across plant cells (**Figure 1C**)¹⁵. Therefore, it is
57 essential to identify additional key sites that significantly influence viral behavior and elucidate the
58 molecular mechanisms of drugs, providing a basis for developing effective and sustainable pest
59 management strategies.

60 In 2019, Podobnik and co-workers reported the structural basis of PVY CP, which
61 demonstrated that the interaction between viral RNA (vRNA) and CP is important for virion to
62 maintain a stable helical configuration¹³. This pioneering work provides opportunities for the design
63 of antiviral agents based on PVY CP. It has been suggested that the conserved residues Ser¹²⁵, Arg¹⁵⁷,
64 and Asp²⁰¹ of PVY CP are related to the binding of vRNA. Hence, using drugs to interfere with
65 these sites may hinder the interaction between CP and vRNA, thereby affecting downstream
66 pathogenic behaviors. Moreover, because these sites belong to conserved regions, this enables the
67 broad spectrum of the drug and makes it less likely to develop drug resistance. Unfortunately, no
68 molecules have yet been discovered to enter this cavity and bind to its sites.

69 Here, we disclose a case of phytovirucide that could form a stable H-bond with Ser¹²⁵ of PVY
70 CP to exert antiviral properties (**Figure 1D**). The present investigation explores a range of
71 innovative compound derivatives of 2,2-dimethyl-2H-chromene that were designed by using a
72 molecular hybridization strategy. Notably, these target compounds bear a unique Schiff base unit
73 and a phenolic hydroxyl group, which introduces additional hydrogen bond donors. This inclusion
74 facilitates the formation of intramolecular hydrogen bonds with nitrogen atoms in neighboring
75 Schiff base units, creating a six-membered ring and enhancing structural stability, as confirmed by

76 X-ray diffraction results (CCDC No. 2297246). Many of our synthesized derivatives displayed
77 potent curative, protective, and inactivating effects against PVY during bioactivity assays. Among
78 them, compound **C50**, identified through constructing a three-dimensional quantitative structure-
79 activity relationship (3D-QSAR) model, demonstrated significantly better inactivation effects (EC_{50}
80 = 53.3 $\mu\text{g}/\text{mL}$) compared to the commercial drug NNM (EC_{50} = 73.7 $\mu\text{g}/\text{mL}$). Combining molecular
81 docking, molecular dynamics simulation, and a range of biological experiments allowed us to
82 discover that compound **C50** can specifically bind to the conserved residue Ser¹²⁵ on CP. We
83 confirmed that this site is crucial for the interaction between vRNA and CP, which can be
84 competitively inhibited by our drug, leading to dysfunction in the assembly of virus particles. Our
85 research enhances knowledge of the mode of action of PVY-targeting drugs and lays the groundwork
86 for designing innovative inhibitors of virus CP assembly at the molecular level.

87 **RESULTS**

88 **Chemistry**

90 Firstly, *p*-phenylenediamine and substituted sulfonyl chloride were reacted in dichloromethane
91 solvent, utilizing triethylamine as an acid scavenger, to synthesize intermediates designated as
92 **A1–A41**; secondly, 2,4-dihydroxybenzaldehyde was used as raw materials with 3-methyl-2-butene
93 or citral, and refluxed in an ethanol solution of triethylamine and anhydrous calcium chloride, and
94 carried out the ring-combining reaction to acquire intermediates **B1** and **B2**. Finally, **A1–A41** and
95 **B1** and **B2** were used as raw materials and heated to reflux with ethanol as a solvent to obtain 2,2-
96 dimethyl-2*H*-chromene derivatives **C1–C50** with sulfonamide units (**Figure 2A**). As X-ray
97 diffraction results showed, the hydroxyl group at the 5-position on the chromene ring of compound
98 **C6** formed an intramolecular hydrogen bonding interaction with the nitrogen atom on the imine unit
99 at the 6-position. This force formed a six-membered ring structure, which led to a more stable
100 structure of the synthesized title compounds of the salicylaldehyde Schiff base class (**Figure 2B**). It
101 is clear that the chemical properties of this class of compounds fully exhibit the *E* configuration.

102 **Assay anti-PVY activity**

104 Utilizing the half-leaf blight method with *Chenopodium amaranticolor* as the indicator host and
105 NNM as the positive control, the anti-PVY efficacy of all target compounds at a concentration of
106 500 $\mu\text{g}/\text{mL}$ was assessed and tabulated in **Table 1**. The target compounds exhibited notable to
107 superior antiviral potency towards PVY, with 13 of the target compounds (**C7, C10, C16, C24, C26,**
108 **C27, C28, C29, C32, C34, C36, C37, C38, and C50**) having curative activities and protective
109 activities in the range of 60–70%, significantly higher than those of the commercial agent NNM
110 (50.1%, 50.3%). Compounds **C6, C26, C27, C32, C40, and C50** showed comparable or better
111 activity than NNM for inactivating effect. Based on the excellent inactivating performance of this
112 group of compounds (inhibition rate around 80%), we determined the EC_{50} values of inactivating
113 activity for all target compounds. We found that target compounds **C6** and **C50** showed better
114 inactivating EC_{50} values of 56.7 $\mu\text{g}/\text{mL}$ and 53.3 $\mu\text{g}/\text{mL}$ compared to the control agent NNM (73.7
115 $\mu\text{g}/\text{mL}$). The inactivating property of compound **C50** at different concentrations is shown in **Figure**
116 **3A**. NNM serves as the positive control, whereas the negative control is positioned on the left flank
117 of the leaf. Given the excellent inactivating activity of **C6** and **C50**, we next studied the preliminary
118 mechanism behind this.

120 **Compound C50 inhibits systemic infection of PVY**

121 To evaluate the effect of **C50** on PVY infection, we infiltrated the *Nicotiana benthamiana*
 122 plants with Agrobacterium carrying the PVY infectious clone pCamPVY-GFP. As depicted in
 123 **Figure 3B**, a notable presence of strong green fluorescence was observed in the stems and apical
 124 shoot leaves of the control group (DMSO, 500 $\mu\text{g}/\text{mL}$). On the other hand, there was a noteworthy
 125 decrease in green fluorescence observed in both the **C50** (500 $\mu\text{g}/\text{mL}$) and NNM (500 $\mu\text{g}/\text{mL}$)
 126 treatment cohorts, with a more substantial reduction observed in the **C50** treatment cohort. Reverse
 127 transcription quantitative real-time polymerase chain reaction (RT-qPCR) analysis revealed that, as
 128 opposed to the control group (in which PVY RNA accumulation was normalized as 100%), the PVY
 129 RNA accumulation level in **C50** and NNM- treated *N. benthamiana* plant was significantly reduced
 130 to 18.9% and 51.8%, respectively, in the systemic leaves of the infected *N. benthamiana* leaves
 131 (**Figure 3C**). The RT-qPCR results for GFP were consistent with that of PVY RNA (**Figure 3D**).
 132 These results showed that **C50** is a potential antiviral agent against PVY.

134 **3D-QSAR studies**

135 Using Compound **C6** as a template, we aligned compounds in the training set and developed
 136 CoMFA and CoMSIA models incorporating the anti-PVY inactivity of the targets. The parameters
 137 of these models were then scrutinized to assess their reliability. **Table 2** displays the q^2 , r^2 , SEE, and
 138 F values of the built CoMFA and CoMSIA models. Both models' q^2 , r^2 , and F values exhibited more
 139 significance than 0.5, 0.8, and 100, respectively. Additionally, the SEE values were comparatively
 140 less, suggesting that the built models possess predictive capabilities. According to the data in
 141 **Figures 4A & 4B** and **Table S1**, the experimental and theoretical pEC₅₀ values closely matched.
 142 The residuals in the analysis had absolute values below 0.3. The linear correlation coefficients for
 143 experimental vs predicted pEC₅₀ were high, at 0.9339 for the CoMFA and 0.9196 for the CoMSIA.
 144 These findings provide further evidence that both CoMFA and CoMSIA models effectively forecast
 145 the anti-PVY activity of the compounds.

146 The CoMFA model showed nearly equal contributions from steric (50.5%) and electrostatic
 147 (49.5%) fields, emphasizing their joint importance for anti-PVY activity. Both factors should be
 148 addressed when optimizing compounds. Based on the CoMFA model, it can be seen that the position
 149 of R¹ is mainly a green module (**Figure 4C**), indicating that increasing the spatial site resistance of
 150 R¹ is advantageous to the anti-PVY inactivating activity, in which substitution of the aromatic ring
 151 with a significant site resistance is better than that of the aliphatic or cycloalkanes with a small site
 152 resistance, such as **C7** (R¹ = 3-FC₆H₄, R² = H, EC₅₀ = 100.3 $\mu\text{g}/\text{mL}$) < **C29** (R¹ = (CH₂)₃CH₃, R² =
 153 H, EC₅₀ = 682.1 $\mu\text{g}/\text{mL}$). Positions are mainly yellow modules, indicating that increasing the spatial
 154 site resistance of R² is detrimental to anti-PVY inactivating activity, such as **C41** (R¹ = 4-ClC₆H₄,
 155 R² = CH₂CHC(CH₃)₂, EC₅₀ = 780.8 $\mu\text{g}/\text{mL}$) > **C6** (R¹ = 4-ClC₆H₄, R² = H, EC₅₀ = 56.7 $\mu\text{g}/\text{mL}$),
 156 **C42** (R¹ = 4-CH₃C₆H₄, R² = CH₂CHC(CH₃)₂, EC₅₀ = 503.2 $\mu\text{g}/\text{mL}$) > **C50** (R¹ = 4-CH₃C₆H₄, R² =
 157 H, EC₅₀ = 53.3 $\mu\text{g}/\text{mL}$), **C48** (R¹ = 3,5-di-FC₆H₃, R² = CH₂CHC(CH₃)₂, EC₅₀ = 716.6 $\mu\text{g}/\text{mL}$) > **C26**
 158 (R¹ = 3,5-di-FC₆H₃, R² = H, EC₅₀ = 100.3 $\mu\text{g}/\text{mL}$). In CoMFA's electrostatic field (**Figure 4D**), R¹'s
 159 dominant red module hints at enhanced anti-PVY activity with electron-withdrawing R¹ groups.
 160 The position of R² is mainly a blue module, indicating that introducing electron-donating groups in
 161 R² can be conducive to raising the anti-PVY inactivating activity. In summary, the R¹ substituent is
 162 an electron-withdrawing group, and the introduction of a large-site-resistance substituent is
 163 beneficial to increase the activity; the reduction of the spatial site resistance of the 2-position methyl

164 group (R^2) of the pyran ring and incorporating an electron-donating group boosts anti-PVY activity.
165 **Figures 4E & 4F** depict the three-dimensional and electrostatic fields belonging to the CoMSIA
166 model. Assessment of color block significance and roles yields conclusions mirroring those of the
167 CoMFA model. The hydrophobic field of the CoMSIA model is displayed in **Figure 4G**. A yellow
168 region surrounds R^1 , indicating that introducing hydrophobic groups promotes the anti-PVY activity
169 of target compounds. In contrast, the white color does the opposite. **Figure 4H** shows the hydrogen
170 bonding receptor field of the CoMSIA model, with a larger red module at the position of the
171 sulfonamide group oxygen atom, suggesting that the hydrogen bonding receptor provided by the
172 sulfonamide double-bonded oxygen favors the anti-PVY activity of the compounds.

173 The analysis conducted using the model above demonstrated that incorporating a sizeable
174 electron-withdrawing group at R^1 and a small electron-donating group at R^2 resulted in a favorable
175 enhancement in the anti-PVY activity belonging to compounds under investigation. Furthermore, it
176 was observed that the presence of a sulfonamide group played a crucial role as a hydrogen-bonding
177 acceptor group (**Figure 4I**).

178

179 **Molecular docking and molecular dynamics simulation**

180 To verify whether the compounds have interaction forces with PVY CP and to find their binding
181 sites, compounds **C6** and **C50** were molecularly docked to PVY CP, respectively, employing ultra-
182 precise XP docking under the Schrödinger software module. Detailed examination of XP docking
183 and MM-GBSA outcomes revealed that detailed examination of XP docking and MM-GBSA
184 outcomes revealed compounds **C6** and **C50** had docking scores of -6.045 and -5.999 with PVY CP,
185 and MM-GBSA results were -34.15 kcal/mol and -34.44 kcal/mol, with low docking scores and free
186 energies of binding, which indicated that **C6** and **C50** were stable in binding to PVY CP. The
187 molecular docking results showed that **C6** penetrated deep into the interior of the active pocket of
188 PVY CP (**Figure S1**), developing one hydrogen bond with residue Ser¹²⁵ of PVY CP with a bond
189 length of 1.91 Å, two hydrogen bonds, and one salt bridge with residue Asp²⁰¹ with bond lengths of
190 2.43 Å, 2.34 Å, and 4.70 Å, and one salt bridge and two π -Cation bonds with residue Arg¹⁸⁸ with
191 bond lengths of 4.02 Å, 3.70 Å, and 4.63 Å. Compounds **C50** and **C6** are structurally distinguished
192 only by methyl and chlorine atoms. The docking results are similar to the **C6** results, showcasing
193 **C50**'s deep penetration into PVY CP's active site. It forms a hydrogen bond with Ser¹²⁵ (2.00 Å),
194 two with Asp²⁰¹, and a salt bridge (4.75 Å, 2.42 Å, 2.38 Å). Additionally, it establishes a salt bridge
195 and π -Cation bond with Arg¹⁸⁸, measuring 3.38 Å and 4.58 Å, respectively (**Figure 5A**). In summary,
196 it can be seen that the compounds **C6** and **C50**, which are highly inactivating activity compounds
197 for PVY, both form strong hydrogen bonding interactions forming hydrogen bonds with Ser¹²⁵ of
198 PVY CP at lengths of 1.91 Å and 2.00 Å.

199 Molecular dynamics trajectory simulations of **C50** with PVY CP were carried out for 100 ns,
200 and then molecular dynamics trajectories were subsequently scrutinized. The conformational
201 stability of RMSD against simulation time is shown in the figure, where smaller fluctuations indicate
202 that stable conformations were obtained for all the complexes. The analysis reveals a stable **C50**-
203 PVY CP complex post-15 ns, indicating system equilibrium (**Figure 5B**). RMSF assesses local
204 protein chain variations, highlighting peaks as areas experiencing the most significant fluctuations
205 in the simulation. As shown in **Figure 5C**, the results showed that the protein displayed significant
206 structural pliability within the residue region 12–35AA and 190–225AA after the binding of **C50** to
207 PVY CP.

208 Throughout the simulation, protein-ligand engagements are tracked and classified into four
 209 primary types: H-bond, hydrophobic forces, ionic linkages, and aqueous bridges. **Figure 5D**
 210 illustrates the pivotal amino acids crucial for **C50** binding to PVY CP protein are Ser¹²⁵, Asn¹²⁷,
 211 Asp²⁰¹, Ala²²⁴, Phe²³³, and Arg²⁴⁸. **Figure 5E** demonstrates the interactions between the specific
 212 amino acids of **C50** and PVY CP in terms of time during the entire trajectory. The outcomes indicate
 213 that amino acid residues Ser¹²⁵, Asp²⁰¹, Ala²²⁴, Phe²³³, Thr²⁴¹, Arg²⁴⁸, and Glu²⁵² have multiple
 214 contacts with the ligand.

215 The ligand torsion diagram outlines the transformation of ligand conformations across rotatable
 216 bonds during the simulation path. The upper portion of **Figure 5F** depicts a 2D illustration of a
 217 ligand, featuring color-coded rotatable bonds. Each bond's torsion is visually represented by a
 218 matching colored dial plot and bar graph. The dial plot in the bottom half of **Figure 5F** illustrates
 219 the torsion's conformational changes during the simulation. The bar graph condenses the dial plot
 220 data, displaying the probability density distribution of the torsion.

221 The above results show that compound **C50** penetrated deep into the conserved folding region
 222 of PVY CP and interacted with amino acid residues such as Ser¹²⁵ and Asp²⁰¹. A strong hydrogen
 223 bonding interaction was formed with Ser¹²⁵ suggesting that Ser¹²⁵ may be the key site for binding
 224 *2H*-chromene derivatives containing sulfonamide structure to PVY CP.

225

226 **Purification of the wild-type protein PVY CP^{wt} and the mutant protein PVY CP^{S125A} and** 227 **microscale thermophoresis assay**

228 PVY CP is involved in various biological functions and is pivotal in the life cycle of PVY.
 229 Hence, it is regarded as a promising candidate protein for antiphytoviral agent screening. The PVY
 230 CP^{wt} encoding sequence was constructed into the expression vector pET-32a (+) using whole gene
 231 synthesis methodology. The resultant plasmid was named pET-PVY CP^{wt}. The codon at position
 232 125 was mutated to Alanine based on the pET-PVY CP^{wt}. The resultant plasmid was named pET-
 233 PVY CP^{S125A}. The PVY CP^{wt} and its mutant CP^{S125A} were expressed and purified according to the
 234 previous protocol. SDS-PAGE results showed that an expected band of about 50 kDa was observed.
 235 After enterokinase digestion and His-tag purification resin, a specific band of about 33 kDa was
 236 observed (**Figure S2**). This result is consistent with the theoretical value¹³.

237 Microscale thermophoresis (MST) serves as a potent technique for quantifying the strength of
 238 interactions occurring between small molecules and their respective ligands^{19, 20}. The binding
 239 strength between specific target drugs and PVY CP^{wt} was investigated *in vitro* using MST, as
 240 depicted in **Figure 5G** and **Figure S3**. This experimental approach aimed to acquire insights into
 241 how target compounds exert their influences against PVY. The findings indicated that the binding
 242 strength of target compounds to PVY CP^{wt} was in line with their effectiveness in anti-PVY. The K_d
 243 values for binding of compounds **C6** and **C50** to PVY CP^{wt} were 4.4 μ M and 1.6 μ M, respectively,
 244 indicating that compounds **C6** and **C50** have a strong affinity for PVY CP, which is superior to
 245 NNM ($K_d = 8.6 \mu$ M). Compound **C42** had low inactivating activity against PVY ($EC_{50} = 503.2$
 246 μ g/mL). Its binding to PVY CP^{wt} was also relatively weak ($K_d = 497.1 \mu$ M). To further confirm that
 247 the serine at position 125 of the PVY CP protein is a key site of action for the binding of PVY by
 248 2,2-dimethyl-2*H*-chromene derivatives containing a sulfonamide unit, the serine at position 125 of
 249 the PVY CP protein was fixed point mutated to an alanine called PVY CP^{S125A}. Similarly, the affinity
 250 of target compounds for interacting with PVY CP^{S125A} was tested. The findings indicated a markedly
 251 diminished binding affinity between the target compounds and PVY CP^{S125A}, such as the K_d value

252 of compound **C50** was decreased from 1.6 μM to 125.4 μM . Among them, the weakening of binding
 253 between NNM and PVY CP^{S125A} was not very obvious, indicating that the serine at position 125 of
 254 PVY CP protein is not a key site for binding of NNM to PVY CP, which further indicates that this
 255 site is the critical site for anti-PVY of 2,2-dimethyl-2*H*-chromene derivatives containing
 256 sulfonamide unit.

257

258 **Effects of mutation at position Ser¹²⁵ of CP on PVY accumulation levels**

259 To further validate the possibility of the residue Ser¹²⁵ of CP function as a potential target site
 260 for the small molecule **C50** *in vivo*, we mutated the codon at position 125 in CP based on the
 261 infectious clone pCamPVY-GFP using site-directed mutagenesis, the resultant plasmid was named
 262 pCamPVY^{S125A}-GFP (the produced virus named as PVY^{S125A}-GFP) (**Figure 6A**). The plasmids
 263 pCamPVY-GFP and pCamPVY^{S125A}-GFP were transformed into *Agrobacterium* GV3101 by freeze-
 264 thawing, respectively. *Agrobacterium* carrying those plasmids were infiltrated on the fully expanded
 265 leaves of four to six-week-old *N. benthamiana* plants. At 7 days post-agroinfiltration (dpai), a strong
 266 green fluorescence was observed on the systemic leaves of *N. benthamiana* plants infiltrated with
 267 *Agrobacterium* carrying pCamPVY-GFP under UV light. However, no green fluorescence was
 268 observed on the *N. benthamiana* plants infiltrated with *Agrobacterium* cells carrying
 269 pCamPVY^{S125A}-GFP (**Figure 6B**). Western blot and RT-qPCR analyses revealed a substantial
 270 accumulation of PVY CP in the systemic leaves of wild-type PVY GFP-infected *N. benthamiana*
 271 plants. In contrast, only minimal traces were detected in the corresponding leaves of PVY^{S125A}-GFP-
 272 infected *N. benthamiana* (**Figures 6C & 6D**). In summary, PVY CP^{S125} significantly affected virus
 273 accumulation in *N. benthamiana*.

274 Virus particle assembly and movement are two critical processes for potyviruses infection. To
 275 test the effect of mutation on the Ser¹²⁵ in CP on PVY cell-to-cell movement, we adjusted the OD₆₀₀
 276 value of *Agrobacterium* cells carrying pCamPVY-GFP and pCamPVY^{S125A}-GFP to 0.5, and then
 277 further diluted 1000 times. The diluted *Agrobacterium* cells was infiltrated on four-to-six-week-old
 278 *N. benthamiana* plants. The cell-to-cell movement was observed using a laser confocal microscope
 279 at 3 dpai. Confocal microscopy analysis showed that PVY could move to multiple cells in the *N.*
 280 *benthamiana* plants inoculated with PVY-GFP. However, the number of cells displaying green
 281 fluorescence was much less in the *N. benthamiana* plants inoculated with PVY^{S125A}-GFP (**Figure**
 282 **6E**). The findings suggested that the PVY CP^{S125} mutation did not impair the cell-to-cell movement
 283 of PVY-GFP.

284 Based on the above experimental results, we found that the substitution of Ser¹²⁵ with Alanine
 285 in CP significantly affected the PVY accumulation in *N. benthamiana* plants but did not abolish its
 286 cell-to-cell movement. Disturbing the interaction between CP and vRNA reduces the stability of the
 287 virus particles. Previous studies have shown that Ser¹²⁵ of CP binds viral RNA¹³. It is interesting to
 288 know whether the mutation on Ser¹²⁵ affects the virus particle assembly. We purified the virus
 289 particles of PVY-GFP and PVY^{S125A}-GFP, respectively, followed by the previously reported
 290 protocol¹⁵. The stability of PVY virus particles is derived from many CP-vRNA interactions, and
 291 Ser¹²⁵ serves as one of the sites where the PVY CP binds to the vRNA. Mutation of this polar amino
 292 acid residue (Ser) to the non-polar amino acid Ala may impact virus particle assembly. Therefore,
 293 we further observed the effect of PVY CP^{S125} on virus particle assembly by transmission electron
 294 microscopy. Wild-type PVY-GFP and mutant PVY CP^{S125A}-GFP were infiltrated into leaves of age-
 295 appropriate *N. benthamiana*, and virus particles were collected for virus particle extraction at 5 dpai.

296 The purified specimens were treated with 1% phosphotungstic acid staining, followed by
297 morphological observation of the refined PVY virus particles via transmission electron microscopy.
298 Intact PVY virus particles, curved linear particles of approximately 11 nm × 680–900 nm in size
299 (**Figure 6G**), were observed in PVY-GFP and PVY-GFP^{S125A}-treated leaves, which is in accordance
300 with literature reports¹⁵. Notably, the viral particle count in PVY^{S125A}-GFP samples was markedly
301 lower than that in PVY-GFP-infected counterparts (**Figure 6F**). Thus, PVY CP^{S125} is essential for
302 forming PVY virus particles in plants.

303

304 DISCUSSION

305 Natural compounds serve as a vital resource in the pursuit of innovative antiviral medications.
306 Among them, 2,2-dimethyl-2*H*-chromene is present in large quantities in nature and possesses a
307 vast range of antiviral activities. Calanolide A, an extract from the tropical rainforest plant
308 *Calophyllum lanigerum*, was one of the first natural products to be discovered with anti-HIV-1
309 activity²¹. Recently, a new indole alkaloid, Isoaspergilline A, has been isolated from the
310 fermentation product of the tobacco endophyte fungus *Aspergillus versicolor* and has been
311 shown to have excellent anti-TMV activity²². Sulfonamide derivatives have always been the star
312 structures in drug discovery and development, which increase the water solubility of drugs and
313 provide additional hydrogen-bonded receptors. Previous work by our group has shown that
314 sulfonamides have excellent antiphytoviral activity, and some of the compounds can bind
315 specifically to CP^{15, 16, 23–26}. Salicylaldehyde Schiff base derivatives (*E*)-2,4-dichloro-6-(((3-
316 methoxyphenyl) imino) methyl) phenol functions as a synthetic elicitor to enhance the immune
317 response of plants. To resist persecution by harmful organisms, salicylaldehyde Schiff base
318 derivatives also have excellent antiviral activity^{27,28}.

319 In drug design, a molecular hybridization strategy is an important approach based on
320 combining two or more molecular fragments with different biological activities into a new
321 molecular entity by chemical or biological means. This strategy aims to combine the individual
322 fragments' strengths to improve the biological activity, pharmacokinetic properties, and selectivity
323 of the new molecule against a specific target^{29,30}. Here, we have developed sulfonamide-containing
324 2*H*-chromene derivatives with anti-PVY activity by a clever combination of a sulfonamide structure
325 that increases the water solubility of the drug and provides an additional hydrogen-bonded receptor
326 and a natural product structure 2,2-dimethyl-2*H*-chromene, which has antiviral activity. Notably,
327 these target compounds carry a unique salicylaldehyde Schiff base unit, as confirmed by X-ray
328 diffraction results, where the phenolic hydroxyl group forms intramolecular hydrogen bonds with
329 nitrogen atoms in the neighboring Schiff base unit to constitute a six-membered ring, which
330 enhances the structural stability of the target compounds. 3D-QSAR plays a crucial role in drug
331 design^{31–33}. This approach employs theoretical modeling and statistical methodologies to
332 investigate the quantitative correlation between the 3D molecular configurations of a compound
333 series and their respective biological outcomes, and it can reveal conformational relationships and
334 guide structural modifications. Once a reliable 3D-QSAR model has been established, it facilitates
335 the prediction of the biological potency of compounds. A 3D-QSAR model was constructed based
336 on the EC₅₀ value of the anti-PVY inactivating activity of this series of compounds, which further
337 guided the synthesis of **C50**. The bioactivity assessment revealed **C50** to exhibit potent anti-PVY
338 efficacy, with an EC₅₀ of 53.3 μg/mL for its inactivating activity, outperforming the standard agent
339 NNM which had an EC₅₀ of 73.7 μg/mL. This led to our interest in the mechanism of antiviral action

340 of **C50**.

341 Currently, there are two primary approaches for tackling plant viral infections. One prominent
342 method is stimulating the host immune system against viral invasion through plant immune inducers
343 ^{24–26, 32, 34}. The other is the use of antiviral drugs, which target the virus's genetic material or essential
344 proteins to stop its pathogenic behavior, a simple mode of action, and a much faster onset of action
345 ^{14–17, 35}. The CP of plant viruses holds a pivotal function throughout the viral lifecycle, including
346 assembly and movement of virus particles, transmission by vectors, and RNA translation and
347 replication, and is a key biochemical target for developing new pesticides ^{14–16, 35, 36}.

348 Moreover, based on the excellent inactivating activity of **C50** against PVY, molecular docking,
349 and molecular dynamics simulations revealed that there is a strong interaction between **C50** and the
350 active pocket in the conserved folding region of the PVY CP, where a segment of the amino acid
351 sequences within the specified area are among all the flexible filamentous viruses highly conserved
352 ^{13, 36, 37}. Thus, scientists consider this a key target for developing antiviral agent drugs ³⁷. Therefore,
353 interfering with these sites using drugs may hinder the interaction between CPs and vRNA, thereby
354 affecting downstream pathogenic behavior. In addition, since these sites are conserved regions, this
355 allows for a broad range of drug action and less likely resistance. What is exciting is that **C50** forms
356 a strong hydrogen bonding interaction with amino acid residue Ser¹²⁵ in the conserved folding
357 region of CP, which serves as one of the key sites for CP binding to vRNA ¹³. It is reasonable to
358 believe that our drug can compete with viral ssRNAs to bind to this site, which leads to dysfunction
359 of viral particle assembly and thus inhibits viral infestation in plants.

360 In the early stages of drug discovery, targeted mutagenesis strategies and MST techniques can
361 be used to validate the effectiveness of potential drug targets ^{15, 20}. The mechanism of action and
362 target selectivity of drug molecules can be initially assessed by altering critical residues of the target
363 protein and observing the attachment of the drug molecule to the mutated target protein. The targeted
364 mutation of Ser¹²⁵ on PVY CP to Ala¹²⁵ combined with MST assay revealed that the attachment of
365 **C50** to PVY CP was noticeably diminished, which further indicates that this site is the critical site
366 for anti-PVY of **C50**.

367 Previous research has demonstrated that the CP of PVY engages with vRNA twice: firstly, at
368 three critical conserved vRNA-binding amino acids, Ser¹²⁵, Arg¹⁵⁷, and Asp²⁰¹, within a structured
369 region; secondly, at a non-conserved site, Ser²⁴⁰, positioned in the C-terminal segment of CPn ¹³.
370 From a functional standpoint, mutations in the conserved Arg and Asp residues of CPs disrupt the
371 in vitro assembly of potyvirus Johnsongrass mosaic virus and hinder the assembly and intercellular
372 trafficking of potyvirus Pepino mosaic virus within plants ^{37, 38}. For PVY, however, there is no
373 information on whether mutations in conserved residues of the CP affect virus function. We
374 successfully expressed and purified a mutant CP (PVY CP^{S125A}) in *E. coli* that mutated Ser at
375 position 125 in the conserved region of the PVY CP to Ala, and this result preliminarily
376 demonstrated that the Ser¹²⁵ mutation did not affect the in vitro assembly of the CP. We constructed
377 the mutant PVY^{S125A}-GFP using a targeted mutagenesis strategy to verify this target's validity and
378 other functions in vivo. Infestation of *N. benthamiana* with *Agrobacterium tumefaciens* containing
379 the PVY^{S125A}-GFP plasmid revealed a considerable decrease in the accumulation of PVY in the
380 plant, the same as that found after drug treatment. The accumulation of plant viruses in the host is
381 mainly influenced by the replicative assembly and movement of virus particles ^{39, 41–43}. Our
382 experimental results by confocal microscopy and analysis indicated that the mutation in the PVY
383 CP^{S125} locus would not impede the intercellular dissemination of PVY. but results in fewer virus

384 particles. The likely reason for this is that the Ser¹²⁵ mutation affects viral assembly, resulting in
385 fewer viral particles being formed.

386

387 **Conclusion**

388 CP is an essential component of utmost utility in viral life cycle, as it unlocks a variety of
389 important downstream pathogenic processes. Efforts in developing effective CP inhibitors with
390 unique action mechanisms continue to the present day; the contribution reported here provides a
391 myriad of 2*H*-chromene-based antiphytovirals that have shown promising abilities against PVY
392 infection. Compound **C50** stood out among the 50 products and control commercial drug. In vitro,
393 the binding site on CP was discovered and verified as Ser¹²⁵ using molecular docking paired with
394 MST. Several tests conducted in vivo indicated that Ser¹²⁵ is important during the mutual effect
395 between PVY CP and vRNA, which is necessary for the assembly of PVY virions. Compound **C50**
396 can dramatically decrease the viral pathogenicity through competitively inhibiting position Ser¹²⁵
397 (**Figure 7**). In conclusion, this study provides a theoretical basis and potential action sites for the
398 development of CP-based virus assembly inhibitory pesticides, offering new avenues for combating
399 plant viral infections.

400

401 **Limitations of the study**

402 Although compounds with good inhibitory activity against PVY were identified, subsequent
403 structural optimization of this class of compounds is required to discover more active and less costly
404 lead small molecules against plant viruses. The antiviral efficacy of **C50** was initially substantiated
405 in this study solely through molecular docking and dynamic simulations, MST and preliminary
406 investigations on the effect of mutated amino acid sites on the function of PVY virus infestation,
407 movement and viral particle formation were carried out. However, whether the drug can make host
408 plants resistant to the disease is still unknown. In addition, changes in the binding affinity of CP to
409 vRNA after Ser¹²⁵ mutation or drug treatment have not been verified by bio-layer interferometry
410 technology.

411

412 **ACKNOWLEDGEMENTS**

413 Thanks to the State Key Program of National Natural Science of China (No. 32330087), the
414 General Program of the National Natural Science Foundation of China (No. 31871933), the National
415 Science Foundation for Young Scientists of China (No. 32302388) and the Central Government
416 Guides Local Science and Technology Development Fund Projects (Qiankehezhongyindi) (No.
417 2024007) for supporting the project.

418 Thanks to the Center of Pharmaceutical Technology of Tsinghua University for supporting
419 Schrödinger software, molecular dynamics simulation, and molecular docking.

420

421 **AUTHOR CONTRIBUTIONS**

422 Conceptualization, Runjiang Song and Xiong Yang; Methodology, Deguo Liu, Chunle Wei and
423 Yanping Tian; Investigation, Xiong Yang, Deguo Liu, Jianzhan Li, and Chunni Zhao; Writing –
424 Original Draft, Xiong Yang; Writing – Review & Editing, Runjiang Song and Yanping Tian;
425 Funding Acquisition, Baoan Song and Runjiang Song; Resources, Baoan Song, Xiangdong Li and
426 Yanping Tian; Supervision, Runjiang Song, and Baoan Song.

427

428 **DECLARATION OF INTERESTS**

429 The authors declare no competing interests.

430

431 **FIGURE TITLES AND LEGENDS**432 **Figure 1. Rational design of 2H-chromene-based antiphytovirals.**

433

434 **Figure 2. Production of the intended compounds.**

435 (A) Manufacturing pathways for the target molecules. Reagent and conditions: (i) Et₃N,
 436 DCM, 0 °C 30 min, then at rt 3 h, 50–80% yield; (ii) Et₃N, CaCl₂, EtOH, reflux, 3 h, 50–60% yield;
 437 (iii) cat. AcOH, MeOH, reflux, 5 h, 40–75% yield. (B) X-ray crystal structure of compound
 438 C6 (CCDC: 2297246).

439

440 **Figure 3. Effect of C50 against PVY infection.**

441 (A) Effect of C50 against PVY infection in *Chenopodium amaranticolor*. Ningnanmycin (NNM)
 442 was used as a control. The concentration was marked below the inoculated leaves. (B) Green
 443 fluorescence expression map of *Nicotiana benthamiana* leaf blades treated with PVY-GFP
 444 infectious C50 and NNM under UV illumination. (C and D) Quantitative assessment of PVY CP and
 445 GFP accumulation in systemically infected leaves of *N. benthamiana* plants at 7 days post-
 446 agroinfiltration (dpi), utilizing RT-qPCR method. After injection of Agrobacterium with
 447 pCamPVY-GFP, a solution of 1% Tween 80 containing C50 (500 µg/mL), NNM (500 µg/mL), and
 448 DMSO (as a control) was sprayed on the leaves of *N. benthamiana*. RT-qPCR normalization was
 449 achieved using EF1α as an internal control. Data are presented as mean ± SD from three biological
 450 replicates per treatment, with statistical significance indicated by different letters (p < 0.05, one-
 451 way ANOVA).

452

453 **Figure 4. 3D-QSAR Analysis.**

454 (A) CoMFA and (B) CoMSIA models for comparing experimental versus predicted pEC₅₀. (C and
 455 D) CoMFA 3D isopotential maps illustrating (C) steric and (D) electrostatic contributions. (E-H)
 456 CoMSIA 3D isopotential maps depicting (E) steric, (F) electrostatic, (G) hydrophobic, and (H)
 457 hydrogen bond acceptor fields. (I) Relationship between structure and anti-PVY activity.

458

459 **Figure 5. Ser¹²⁵ is a key target for binding compound C50 to PVY CP.**

460 (A) Computational binding analysis of C50 to PVY CP using molecular docking techniques. (B-F)
 461 Comprehensive results of molecular dynamics simulations of C50 and PVY CP. (B) RMSD analysis,
 462 (C) RMSF analysis, (D and E) Interaction analysis, (F) Ligand torsion diagram. (G) analysis
 463 comparing the binding of PVY CP^{wt} and PVY CP^{S125A} mutant proteins to compounds

464

465 **Figure 6. Effect of mutation on Ser¹²⁵ in CP on PVY infection.**

466 (A) Illustrative representation of the pCamPVY-GFP genome structure, highlighting the Ser¹²⁵
 467 residue (marked by red arrows) within the core domain of PVY CP. The blue-bordered box
 468 encapsulates the site-specific mutants, wild-type plasmids, viruses, and their respective sequences.
 469 (B) Comparative visualization of disease symptoms (top) and green fluorescent expression (bottom)
 470 under UV illumination in *N. benthamiana* leaves inoculated with wild-type and mutated PVY strains.
 471 (C and D) Quantitative assessment of PVY CP accumulation in systemically infected leaves of *N.*

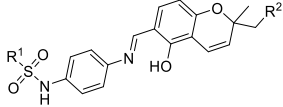
472 *benthamiana* plants at 7 dpai, utilizing RT-qPCR (C) and Western blot (D) methods. RT-qPCR
 473 normalization was achieved using EF1 α as an internal control, while Ponceau S-stained RuBisCO
 474 served as a loading control. Data are presented as mean \pm SD from three biological replicates per
 475 treatment, with statistical significance indicated by different letters ($p < 0.05$, one-way ANOVA).
 476 (E) Examination of cell-to-cell movement dynamics in *N. benthamiana* plants infected with wild-
 477 type and mutated PVY strains at 3 dpai. (F) Enumeration of PVY particles within 70 μm^2
 478 microscopic fields, presented as mean \pm SD derived from five fields per treatment. Statistical
 479 significance is denoted by different letters ($p < 0.05$, one-way ANOVA). (G) Particles of PVY-GFP,
 480 and PVY^{S125A}-GFP under transmission electron microscope.

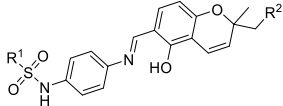
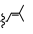
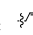
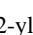
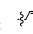
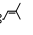
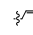
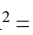
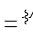
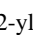
481

482 **Figure 7. Mechanism of anti-PVY action of compound C50.**

483

484 **TABLE TITLES AND LEGENDS**485 **Table 1. Antiviral efficacies of target compounds directed against PVY.**

Compd.		Curative activity (%) ^a	Protective activity (%) ^a	Inactivating activity (%) ^a	EC ₅₀ for inactivating activity ($\mu\text{g/mL}$)
C1	R ¹ = 4-OCH ₃ C ₆ H ₄ , R ² = H	50.7 \pm 5.5	62.2 \pm 6.1	55.1 \pm 6.0	441.2 \pm 5.2
C2	R ¹ = 4-CF ₃ C ₆ H ₄ , R ² = H	63.1 \pm 5.8	58.9 \pm 3.5	71.5 \pm 3.5	255.7 \pm 7.2
C3	R ¹ = (CH ₂) ₇ CH ₃ , R ² = H	12.3 \pm 2.1	39.4 \pm 3.7	40.1 \pm 3.0	605.1 \pm 12.2
C4	R ¹ = Thiophene-2-yl, R ² = H	28.1 \pm 1.7	29.3 \pm 2.9	38.1 \pm 3.1	667.3 \pm 20.1
C5	R ¹ = 4-FC ₆ H ₄ , R ² = H	70.3 \pm 5.8	63.0 \pm 1.6	66.7 \pm 6.4	165.3 \pm 8.7
C6	R ¹ = 4-ClC ₆ H ₄ , R ² = H	63.1 \pm 2.1	57.3 \pm 3.5	80.0 \pm 1.9	56.7 \pm 4.2
C7	R ¹ = 3-FC ₆ H ₄ , R ² = H	73.7 \pm 2.6	70.2 \pm 2.6	74.9 \pm 2.4	100.3 \pm 5.7
C8	R ¹ = 2-FC ₆ H ₄ , R ² = H	67.7 \pm 2.0	58.4 \pm 3.7	58.9 \pm 2.6	369.2 \pm 9.9
C9	R ₁ = Pyridin-3-yl, R ² = H	30.4 \pm 2.9	32.7 \pm 3.5	60.1 \pm 2.7	310.2 \pm 8.6
C10	R ¹ = 5-Br-Thiophene-2-yl, R ² = H	68.1 \pm 3.0	63.3 \pm 4.4	50.2 \pm 2.4	492.3 \pm 13.3
C11	R ¹ = 3-CNC ₆ H ₄ , R ² = H	29.1 \pm 6.1	26.7 \pm 3.7	44.2 \pm 4.6	703.3 \pm 25.3
C12	R ¹ = 4-NO ₂ C ₆ H ₄ , R ² = H	31.8 \pm 3.9	31.9 \pm 3.9	58.9 \pm 4.9	400.3 \pm 7.5
C13	R ¹ = Cyclopropane, R ² = H	33.4 \pm 3.5	27.8 \pm 3.5	49.1 \pm 3.1	531.2 \pm 20.7
C14	R ¹ = 2,5-di-ClC ₆ H ₃ , R ² = H	31.2 \pm 4.1	28.6 \pm 2.4	35.2 \pm 2.8	751.1 \pm 19.4
C15	R ¹ = 2,5-di-FC ₆ H ₃ , R ² = H	54.1 \pm 2.8	54.6 \pm 3.1	30.7 \pm 2.7	903.2 \pm 14.3
C16	R ¹ = 3-BrC ₆ H ₄ , R ² = H	61.2 \pm 2.8	63.4 \pm 3.1	41.1 \pm 1.5	688.4 \pm 17.2
C17	R ¹ = C ₆ H ₅ , R ² = H	56.8 \pm 5.6	61.2 \pm 2.9	74.3 \pm 1.8	168.4 \pm 4.8
C18	R ¹ = 4-CH ₃ CH ₂ C ₆ H ₄ , R ² = H	57.4 \pm 4.3	59.0 \pm 2.9	79.1 \pm 1.2	202.1 \pm 3.8
C19	R ¹ = 2,4,6-tri-CH ₃ -C ₆ H ₂ , R ² = H	25.8 \pm 2.6	58.7 \pm 3.5	56.7 \pm 1.9	492.3 \pm 11.2
C20	R ¹ = 4-tert-butylC ₆ H ₄ , R ² = H	32.4 \pm 5.8	24.5 \pm 2.2	20.1 \pm 2.5	1003.4 \pm 18.2
C21	R ¹ = 4-CH ₃ CONHC ₆ H ₄ , R ² = H	25.7 \pm 2.6	22.7 \pm 2.9	33.5 \pm 2.1	1021.3 \pm 20.7
C22	R ¹ = 2-CF ₃ C ₆ H ₄ , R ² = H	50.2 \pm 2.9	53.7 \pm 2.0	45.7 \pm 2.0	587.0 \pm 9.9
C23	R ¹ = 3,5-di-ClC ₆ H ₃ , R ² = H	19.1 \pm 3.2	28.0 \pm 2.7	23.4 \pm 1.4	870.9 \pm 17.3
C24	R ¹ = 5-Cl-Thiophene-2-yl, R ² = H	67.6 \pm 3.1	65.8 \pm 2.9	34.5 \pm 2.3	753.6 \pm 10.3
C25	R ¹ = 2-ClC ₆ H ₄ , R ² = H	56.8 \pm 5.0	70.9 \pm 4.0	67.3 \pm 2.7	243.9 \pm 10.2
C26	R ¹ = 3,5-di-FC ₆ H ₃ , R ² = H	65.2 \pm 2.0	63.7 \pm 2.9	81.3 \pm 3.8	100.3 \pm 4.5
C27	R ¹ = 3-CH ₃ C ₆ H ₄ , R ² = H	63.5 \pm 3.0	68.7 \pm 3.5	81.8 \pm 3.3	90.3 \pm 7.1
C28	R ¹ = Benzyl, R ² = H	64.4 \pm 3.3	68.9 \pm 2.3	47.5 \pm 1.2	503.1 \pm 12.8
C29	R ¹ = (CH ₂) ₃ CH ₃ , R ² = H	64.2 \pm 2.3	66.6 \pm 4.5	35.9 \pm 5.0	682.1 \pm 10.0

Compd.		Curative activity (%) ^a	Protective activity (%) ^a	Inactivating activity (%) ^a	EC ₅₀ for inactivating activity (μg/mL)
C30	R ¹ = 4-OCF ₃ C ₆ H ₄ , R ² = H	31.0 ± 2.6	39.6 ± 6.2	32.2 ± 4.7	834.1 ± 18.3
C31	R ¹ = 2,4-di-ClC ₆ H ₃ , R ² = H	29.1 ± 2.4	39.7 ± 6.2	35.6 ± 4.7	975.7 ± 20.0
C32	R ¹ = 2,6-di-FC ₆ H ₃ , R ² = H	66.8 ± 2.2	63.4 ± 6.0	80.9 ± 3.6	88.3 ± 4.0
C33	R ¹ = 2-BrC ₆ H ₄ , R ² = H	52.1 ± 0.6	34.6 ± 3.6	78.1 ± 5.1	139.2 ± 3.2
C34	R ¹ = 4-BrC ₆ H ₄ , R ² = H	66.4 ± 2.9	65.2 ± 5.3	79.5 ± 3.9	147.3 ± 8.3
C35	R ¹ = 3-CF ₃ C ₆ H ₄ , R ² = H	48.6 ± 2.6	64.3 ± 4.2	29.2 ± 3.3	803.0 ± 12.3
C36	R ¹ = 3-ClC ₆ H ₄ , R ² = H	68.5 ± 4.9	61.0 ± 2.3	44.4 ± 2.0	557.2 ± 14.3
C37	R ¹ = 2-F-3-ClC ₆ H ₃ , R ² = H	63.1 ± 3.5	60.2 ± 2.3	59.5 ± 4.2	306.3 ± 11.0
C38	R ¹ = 2-CH ₃ -3-ClC ₆ H ₃ , R ² = H	65.5 ± 3.0	61.1 ± 3.1	64.0 ± 3.3	410.3 ± 9.7
C39	R ¹ = 2,5-di-CH ₃ -Isoxazol-4-yl, R ² = H	41.0 ± 2.7	47.8 ± 4.4	63.1 ± 3.1	397.1 ± 2.3
C40	R ¹ = <i>L</i> (-)-10-Camphoryl, R ² = H	60.2 ± 3.8	53.2 ± 1.8	81.2 ± 1.8	204.3 ± 7.1
C41	R ¹ = 4-ClC ₆ H ₄ , R ² = 	34.2 ± 4.7	36.9 ± 2.2	36.5 ± 1.5	780.8 ± 15.3
C42	R ¹ = 4-CH ₃ C ₆ H ₄ , R ² = 	38.8 ± 3.3	44.5 ± 3.4	52.2 ± 3.5	503.2 ± 17.0
C43	R ¹ = 5-Cl-Thiophene-2-yl, R ² = 	33.1 ± 3.7	40.1 ± 2.8	39.7 ± 3.8	512.3 ± 11.0
C44	R ¹ = 3-CH ₃ C ₆ H ₄ , R ² = 	29.7 ± 6.3	40.0 ± 1.7	34.0 ± 2.8	881.7 ± 17.3
C45	R ¹ = 3-F C ₆ H ₄ , R ² = 	32.1 ± 1.4	42.4 ± 2.4	32.7 ± 3.3	515.9 ± 9.0
C46	R ¹ = 4-CF ₃ C ₆ H ₄ , R ² = 	33.5 ± 2.1	41.1 ± 3.8	49.4 ± 3.1	522.4 ± 8.1
C47	R ¹ = 2,6-di-FC ₆ H ₃ , R ² = 	30.7 ± 4.9	37.1 ± 2.7	44.7 ± 1.2	629.5 ± 11.2
C48	R ¹ = 3,5-di-FC ₆ H ₃ , R ² = 	34.7 ± 1.1	31.9 ± 2.7	23.3 ± 2.2	716.6 ± 17.8
C49	R ¹ = 5-Br-Thiophene-2-yl, R ² = 	36.2 ± 1.1	39.4 ± 2.6	40.4 ± 3.3	552.7 ± 9.3
C50	R ¹ = 4-CH ₃ C ₆ H ₄ , R ² = H	68.7 ± 3.8	70.1 ± 1.7	84.1 ± 1.0	53.3 ± 4.3
NNM ^b	/	50.1 ± 2.9	50.7 ± 1.8	82.5 ± 1.3	75.7 ± 4.0

486 ^a Average of three replicates. ^b Ningnanmycin (NNM) used as positive control.

487

488 **Table 2. Statistical outcomes belong to the CoMFA and CoMSIA models.**

Statistical parameter	CoMFA	CoMSIA	Validation criterion
q ²	0.602	0.619	>0.5
ONC	5	4	
r ²	0.984	0.936	>0.8
SEE	0.042	0.081	
F	408.575	127.810	
Fraction of field contributions			
steric	0.505	0.106	
electrostatic	0.495	0.164	
hydrophobic		0.221	
hydrogen-bond donor		0.349	
hydrogen-bond acceptor		0.160	

489

490 STAR METHODS

491 **Resource availability**

492 **Lead contact**

493 Further information and requests for resources and reagents should be directed to and will be
494 fulfilled by the lead contact, Prof. Runjiang Song (songrj@gzu.edu.cn).

495

496 **Materials availability**

497 Plasmids generated in this study are available from the lead contact, Prof. Runjiang Song
498 (songrj@gzu.edu.cn).

499

500 **Data and code availability**

501 All requested data is shared promptly upon receipt of a request.

502 The current study does not encompass the development or reporting of novel coding
503 methodologies.

504 Additional details necessary for re-examination of the data presented in this article can be
505 sourced from the lead contact upon submission of a request.

506

507 **METHOD DETAILS**

508 **Materials and instruments**

509 2,4-dihydroxybenzaldehyde, 3-methylbut-2-enal, citral, *p*-phenylenediamine, and substituted
510 sulfonyl chloride were purchased from Energy Chemical (Anqing, Anhui, China). The solvents
511 employed as reagents were of a grade suitable for direct use, without the necessity for any additional
512 purification steps. A greenhouse was used to cultivate *Nicotiana tabacum* cv. K326, *Nicotiana*
513 *benthamiana*, and *Chenopodium amaranticolor* plants maintained at a 6/18-h (dark/light)
514 photoperiod and 25 °C. PVY were propagated in *N. tabacum* cv. K326.

515 A micro melting point apparatus (XGE X4B) was utilized to ascertain the melting point of the
516 compounds. The ¹H, ¹³C, and ¹⁹F spectra were acquired on Bruker AG 400 and a 500 MHz NMR
517 apparatus, respectively, employing TMS as the internal reference and DMSO-*d*₆ as the solvent
518 medium. High-resolution mass spectrometry (HRMS), facilitated by the Thermo Scientific Q
519 Exactive instrument (Waltham, MA, U.S.A.), was employed to determine the molecular weights of
520 the compounds. Furthermore, X-ray crystallographic data were collected using a Bruker Smart Apex
521 CCD area detector diffractometer (Bruker, Germany), which utilized Mo *K*α radiation for precise
522 measurements.

523

524 **Preparation of compounds C1–C50**

525 The synthesis of intermediate compounds **A1–A41** was achieved by adapting the methodology
526 documented in literature source ⁴³. In a 100 mL round-bottom flask, *p*-phenylenediamine (3 mmol)
527 was dissolved in 20 mL of dichloromethane while being maintained under an ice-bath condition.
528 Triethylamine (4.5 mmol), serving as an acid scavenger, was subsequently added. A solution of
529 substituted sulfonyl chloride (3.00 mmol) in 5 mL of dichloromethane was then slowly dripped into
530 the mixture. Following the completion of the addition, the ice bath was removed, and the reaction
531 was allowed to proceed with stirring for 3 h. The resulting mixture was concentrated and
532 subsequently purified via silica gel column chromatography, employing a mixture of petroleum
533 ether and ethyl acetate (3:1 ratio) as the eluent. This purification process yielded the intermediate
534 compounds **A1–A41**.

535 Intermediate compounds **B1** and **B2** were prepared by adapting and partially refining a
536 literature-based procedure ⁴⁴. In this synthesis, 3-methyl-2-butenal or citral (103.6 mmol), CaCl₂

537 (43.0 mmol), and triethylamine (172.1 mmol) were dissolved in 200 mL of absolute ethanol.
538 Subsequently, 2,4-dihydroxybenzaldehyde (51.8 mmol) was introduced into the solution.
539 Formaldehyde (51.8 mmol) was then added, and the reaction mixture was subjected to reflux for 3
540 h. Following this, the ethanol was removed via vacuum distillation. To the residue, 100 mL of
541 distilled water was added, and the pH was adjusted to 5 using dilute HCl. The aqueous mixture was
542 then extracted with ethyl acetate (three times with 100 mL each). The combined organic extracts
543 were washed with saturated brine, dried over anhydrous MgSO₄, and concentrated. Finally, the
544 crude product was purified by silica gel column chromatography, employing a mixture of petroleum
545 ether and ethyl acetate (30:1) as the eluent, yielding the desired intermediates **B1** and **B2**.

546 Target compounds **C1–C50** were synthesized through the same method and procedure, with
547 **C1** as a representative example, a solution of *N*-(4-aminophenyl)-4-methoxybenzenesulfonamide (1
548 mmol) and intermediate **B1** (1.2 mmol) was prepared by dissolving them in 10 mL of ethanol. A
549 catalytic quantity of glacial acetic acid was then added and then heated. The reaction progress was
550 monitored during the experiment using thin-layer chromatography. Once a significant portion of the
551 starting materials had undergone a reaction, the solvent in the mixture was concentrated. After the
552 evaporation of ethanol and subsequent aqueous workup, the obtained residue underwent purification
553 through column chromatography. This process utilized a solvent system consisting of ethyl acetate
554 and petroleum ether in a ratio of 5:1 as the eluent. This purification process ultimately yielded the
555 target compound **C1**. (*E*)-*N*-(4-(((5-hydroxy-2,2-dimethyl-2*H*-chromen-6-yl) methylene) amino)
556 phenyl)-4-methoxybenzenesulfonamide (**C1**): Yield: 60.13%; yellow solid; m. p. 139–141 °C; ¹H
557 NMR (500 MHz, DMSO-*d*₆) δ 14.25 (s, 1H, -OH), 10.25 (s, 1H, -SO₂NH-), 8.76 (d, *J* = 4.1 Hz, 1H,
558 -N=CH-), 7.73 – 7.67 (m, 2H, Ar-H), 7.34 – 7.26 (m, 3H, Ar-H), 7.14 (dd, *J* = 9.2, 3.6 Hz, 2H, Ar-
559 H), 7.09 – 7.03 (m, 2H, Ar-H), 6.63 (d, *J* = 10.5 Hz, 1H, Ar-H), 6.38 (d, *J* = 7.9 Hz, 1H, Ar-H), 5.72
560 (d, *J* = 10.8 Hz, 1H, Ar-H), 3.79 (d, *J* = 4.2 Hz, 3H, -OCH₃), 1.39 (s, 6H, -CH₃). ¹³C NMR (126
561 MHz, DMSO-*d*₆) δ 163.0, 162.4, 158.6, 157.3, 143.5, 136.9, 134.1, 131.5, 129.4, 129.2, 122.3, 121.4,
562 116.0, 114.9, 113.3, 109.05, 108.4, 77.6, 56.1, 28.3. HRMS (ESI) *m/z* for C₂₅H₂₄N₂O₅S [M+H]⁺
563 calcd 465.14787, found 465.14771.

564 The spectral profiles of all target compounds are provided in the accompanying Supporting
565 information (see Data S2).

566

567 Antiviral bioassay

568 According to previous reports⁴⁵, PVY was infested in *Nicotiana tabacum* K326, and PVY was
569 harvested and purified after showing severe infection symptoms on the leaves. The literature-guided
570 protocol was followed to assess the curative, prophylactic, and non-reactive potential of the target
571 compounds under investigation¹⁵.

572 *Curative Activity of Compounds Against PVY*: To assess the curative effectiveness against PVY,
573 a uniform layer of 200–300 mesh emery was applied to the leaves of *C. amaranticolor*, followed
574 by rubbing with a virus solution. For 1.5 h, then the emery was washed off with water. After the
575 leaves naturally dried, a 500 μg/mL solution of the test compound was carefully applied to one side
576 of the leaf, while the opposite side received a 1% Tween 80 solution as a control. The plants were
577 subsequently incubated in a greenhouse maintained at 25 °C. After 5–7 d, the presence of necrotic
578 spots on the leaves was recorded, with each compound tested on three replicate plants. The average
579 inhibition rate was determined by analyzing the data from these replications.

580 *Protective Activity of Compounds Against PVY*: A 500 μg/mL solution of the targeted

581 compound was delicately applied to one side of *C. amaranticolor* leaves, while the other side was
582 treated with a 1% Tween 80 aqueous solution. The plants were positioned in a greenhouse set at
583 25 °C. Following a 24 h period, the entire leaf surface was inoculated with PVY by uniformly
584 distributing 200–300 mesh emery. After 1.5 h, the emery was washed off with water, and the plants
585 were returned to the greenhouse. After 5–7 d, the number of necrotic spots was tallied, with the
586 assessment based on the greenhouse population. Each compound was tested in triplicate, and the
587 average inhibition rate was subsequently calculated.

588 *Inactivating Activity of Compounds Against PVY:* Target compound solution (1,000 µg/mL)
589 and 2 × virus solution were combined in equal quantities and incubated for 30 min. Evenly distribute
590 emery onto the leaf blades, and apply the mixture of virus and compound solution onto the right
591 side of *C. amaranticolor* leaf blades. Following this, an identical quantity of a 1 × virus solution was
592 applied to the untreated side of the leaf. Following a duration of 1.5 h, the emery residue present on
593 the leaf surface was removed using a rinsing process utilizing water. The plants were incubated
594 within a controlled greenhouse environment, maintaining a consistent temperature of 25 °C. After
595 5–7 d, they proceeded to statistics the number of necrotic spots on the leaves. For each chemical,
596 triplicate experiments were undertaken, and the average percentage of inhibition was subsequently
597 determined.

598

599 **3D-QSAR studies**

600 The software SYBYL-2.1 was used to produce comparative molecular field analysis (CoMFA)
601 and comparative molecular similarity index analysis (CoMSIA) models. A total of 39 compounds
602 were randomly chosen for training purposes, with the remaining 10 exclusively assigned for testing.
603 3D-QSAR models for the molecular structures of the target compounds and their effects on
604 inactivating PVY were developed using partial least squares (PLS) regression. Initially, the
605 structures of the target compounds were subjected to energy minimization within the software.
606 Subsequently, compound **C6** served as the reference molecule, and the 3D conformations of all
607 compounds in the training set were aligned by selecting the common scaffold. Cross-validation of
608 the training set compounds was performed using the leave-one-out strategy (LOO) diligently. This
609 process involved computing the cross-validation coefficient (q^2) and determining the optimal
610 number of principal components (ONC). The model's performance was assessed in terms of its
611 goodness of fit, non-cross-validation coefficient (r^2), Fisher statistic (F), standard error of estimate
612 (SEE), and relative force field contribution. Subsequently, the model was further refined through
613 the conformational search technique. Finally, the optimized model was employed to predict the
614 biological activities of the target compounds in the test set.

615

616 **Molecular docking and molecular dynamics simulation**

617 The molecular docking was performed using the Schrödinger Maestro 13.5 program (March
618 2023 edition). The crystallographic structure corresponding to PVY CP (PDB ID: 6HXX) was
619 initially obtained from the RCSB PDB database. The protein crystals that were obtained underwent
620 a series of protein preprocessing procedures, which included restoring natural ligand states, refining
621 hydrogen bond assignments, minimizing the energy of protein, and eliminating water molecules.
622 The LigPrep module was utilized to process the two-dimensional structure files of compounds **C6**
623 and **C50**, generating all conceivable three-dimensional chiral conformations. The ligand molecules
624 **C6** and **C50** were submitted to molecular docking with the active site of PVY CP utilizing the

625 maximum precision XP docking method. The lower score signifies a diminished binding free energy
626 between the chemical compound and the protein, implying a heightened binding stability.

627 To enhance the binding efficacy of compound-protein complexes, we employed conventional
628 molecular dynamics simulations through the Desmond software. The OPLS4 force field was utilized
629 to accurately model the interactions between the protein and small molecules, while the SPCE model
630 was adopted for the water solvent. The complex was immersed in a cubic water box and fully
631 solvated. To ensure system neutrality, 0.150 M chloride and sodium ions were added. An initial
632 energy minimization was conducted using the steepest descent method, involving 50,000 steps.
633 Following this, the heavy atoms were restrained during NVT and NPT equilibration phases,
634 spanning another 50,000 steps. Throughout, the system temperature was held at 300 K and the
635 pressure at 1 bar. Upon completion of these equilibration stages, an unrestrained simulation was
636 executed for a duration of 100 nanoseconds. The interactions were scrutinized, and dynamic
637 trajectory data was compiled using Maestro 13.5, facilitating further analysis and optimization of
638 the binding mode.

639

640 **Plasmid construction and site-directed mutagenesis**

641 The pCamPVY-GFP plasmid (GenBank accession: MN381731) was constructed in the
642 previous study ⁴⁶. Subsequently, the coding region of PVY CP was amplified via PCR from the
643 pCamPVY-GFP and fused into a modified pCambia0390 vector, which harbors a 35S promoter and
644 the GFP gene, yielding the pCamGFP-PVY CP construct. For expression in *Escherichia coli*, the
645 PVY CP sequence was transferred into the pET-32a (+) vector, creating the pET-PVY CP plasmid.
646 Furthermore, to introduce a Ser¹²⁵ substitution in both pCamPVY-GFP and pET-PVY CP, site-
647 directed mutagenesis was employed, adhering to a previously established protocol ⁴⁷. This led to the
648 generation of pCamPVY^{S125A}-GFP and pET-PVY CP^{S125A} constructs, respectively. All the
649 constructed plasmids were sequenced. **Table S2** lists the primers used in this study.

650

651 **Agrobacterium infection of PVY-GFP, agent treatment, and photographing**

652 The *Nicotiana benthamiana* plants were subjected to infestation by *Agrobacterium tumefaciens*,
653 which carried either pCamPVY-GFP or an empty vector (mock). Following this a solution with
654 target compound **C50** (500 µg/mL), NNM (500 µg/mL), and a volume equivalent to DMSO (serving
655 as the control) was applied via spraying onto all of the leaves. At 7 dpai, the leaves of *N.*
656 *benthamiana* were looked at for the GFP using a LUYOR UV light (Shanghai, China), and captured
657 in photographs. The foliage was gathered, rapidly frozen with liquid nitrogen, and subsequently
658 preserved in a refrigerator set at a temperature of -80 °C.

659

660 **RNA extraction, cDNA synthesis, and RT-qPCR**

661 Leaf blades of *Nicotiana benthamiana* were pulverized into fine powder with the aid of liquid
662 nitrogen, followed by the extraction of total RNA from the leaf tissue utilizing Trizol reagent
663 (Invitrogen, California, USA). Subsequently, cDNA synthesis was conducted through reverse
664 transcription with primers and a reverse transcription kit (Vazyme, Nanjing, China). Any potential
665 DNA contamination was effectively removed using a gDNA wipe enzyme (Vazyme, Nanjing, China)
666 as per the manufacturer's guidelines. RT-qPCR analysis was carried out employing TB Green
667 (TaKaRa, Beijing, China). Detailed information regarding the primers utilized in this investigation
668 can be found in **Table S2**.

669

670 Expression and purification of PVY CP and PVY CP mutants

671 The PVY CP^{wt} gene, the wild-type variant of the Potato Virus Y coat protein, was cloned into
672 the pET-32a (+) prokaryotic expression vector. This recombinant vector was then thermally
673 transformed into BL21(DE3) bacterial host cells for subsequent protein expression. The strains
674 above were cultivated on a liquid Luria-Bertani medium (180 rpm, 37 °C). To initiate the expression
675 of PVY CP, isopropyl β -D-1-thiogalactopyranoside (IPTG) was added to the culture medium at a
676 concentration of 1.0 mmol when the optical density at 600 nm (OD₆₀₀) reached a range between 0.6
677 and 0.8. This step triggered the production of the PVY CP protein. The induction process was
678 maintained for 10 h (180 rpm, 16 °C). The 6 × -His-S-tagged PVY CP^{wt} were purified using nickel-
679 nitriloacetic acid by high-performance column affinity chromatography. Subsequently, enterokinase
680 was employed to digest the proteins, and the desired target proteins were isolated using His-tag
681 purification resin. Ultimately, the proteins were identified through the employment of a 12% sodium
682 dodecyl sulfate-polyacrylamide gel electrophoresis method. The pET-32a (+) plasmid containing
683 the PVY CP^{wt} gene was used as a template. The gene encoding serine at position 125 on PVY CP^{wt}
684 was a point mutation to the alanine gene. The mutant protein was purified using the method for the
685 purification of PVY CP^{wt}, which was PVY CP^{S125A}.

686

687 MST assay for the affinity of the compounds with PVY CP

688 The proteins' binding affinity with target chemicals was evaluated using a Monolith NT.115
689 instrument (Nano Temper, Munich, Germany), utilizing established methods described in
690 literature^{35, 48}. A concentration of 2.0 mM was selected for the chemicals, and the proteins were
691 tagged with the Monolith TM RED-NHS second-generation labeling kit. The MST assay analyzed
692 the fluorescence intensity of the labeled proteins, focusing on a range from 400 to 1200 to
693 investigate their interactions. The scanning method was conducted using an “LED power” setting
694 of 40% and a temperature that was maintained at 25.0 °C.

695

696 Western blot assay

697 The leaves of the assayed *N. benthamiana* were used to extract total protein according to the
698 previously described¹⁵. An anti-GFP (Proteintech, Wuhan, China) or anti-PVY CP (Youke,
699 Shanghai, China) antibody and horseradish peroxidase-conjugated goat anti-rabbit IgG (Proteintech,
700 Wuhan, China) were individually used as the primary and secondary antibody. The visualization of
701 the target protein's signal was facilitated through the use of the Chemi Doc MP Imaging System
702 manufactured by Bio-Rad.

703

704 Virus particle purification

705 Leaves of *N. benthamiana* that had been infected with wild-type or mutated PVY for 5 days
706 were harvested for the extraction of viral particles. The methodology for purifying virion particles
707 was performed according to our established protocol. The supernatant containing PVY was absorbed
708 onto a copper grid coated with a carbon support film (Zhongjingkeyi, Beijing, China) and
709 subsequently stained with a 1% phosphotungstic acid buffer. Subsequently, the structure of PVY
710 particles was visualized using transmission electron microscopy (TEM, Talos F200C, FEI, USA).

711

712 Confocal microscopy

713 To analyze cell-to-cell movement of PVY-GFP and its mutant in *N. benthamiana* plants, the
 714 leaf patches infiltrated with *Agrobacterium* carrying pCamPVY-GFP and pCamPVY^{S125A}-GFP were
 715 observed using a confocal microscope (Carl Zeiss, Germany). The excitation wavelength for
 716 observing GFP fluorescence was adjusted to 488 nm, while the emission wavelengths were specified
 717 to fall within the 520 to 540 nm range. The captured images were subsequently analyzed and
 718 processed with ZEN 2.1 software.

719

720 QUANTIFICATION AND STATISTICAL ANALYSIS

721 All experiments were conducted with three independent biological replicates per treatment.
 722 The sample size (n) for each measurement was determined in triplicate. Statistical analysis was
 723 performed using Microsoft Excel 2021. In **Table 1** all data are presented as means \pm Standard
 724 deviation (SD). SPSS software (version 26.0) was used for one-way ANOVA. Error bars on **Figure**
 725 **3C, 3D, 6C** and **6F** indicate SD. Different letters indicate statistically significant differences ($p <$
 726 0.05).

727

728 SUPPLEMENTAL INFORMATION

729 Document S1. Figures S1–S3, Table S1 and S2, Data S1 and S2

730

731 REFERENCES

- 732 1. Sampaio, S. L., Petropoulos, S. A., Alexopoulos, A., Heleno, S. A., Buelga, C. S., Barros, L.,
 733 Ferreira, I. C. F. R. (2020). Potato peels as sources of functional compounds for the food
 734 industry: A review. *Trends Food Sci. Technol.* *103*, 118–129. 10.1016/j.tifs.2020.07.015.
- 735 2. Rajni, S., Sukhpreet, K., Poonam, A., Atul, D., Priyanka, S. (2023). Conventional and emerging
 736 innovative processing technologies for quality processing of potato and potato-based products:
 737 A review. *Food Control* *153*, 109933. 10.1016/j.foodcont.2023.109933.
- 738 3. Yuen, J. (2021). Pathogens which threaten food security: *Phytophthora infestans*, the potato late
 739 blight pathogen. *Food Secur.* *13*, 1–7. 10.1007/s12571-021-01141-3
- 740 4. Yang, X., Li, Y., Wang, A. (2021). Research advances in potyviruses: From the laboratory bench
 741 to the field. *Annu. Rev. Phytopathol.* *59*, 1–29. 10.1146/annurev-phyto-020620-114550.
- 742 5. Godfray, H. C. J., Beddington, J. R., Crute, I. R., Haddad, L., Lawrence, D., Muir, J. F., Pretty, J.,
 743 Robinson, S., Thomas, S. M., Toulmin, C. (2010). Food security: The challenge of feeding 9
 744 billion people. *Science* *327*, 812–818. 10.1126/science.1185383.
- 745 6. Mburu, H., Cortada, L., Haukeland, S., Ronno, W., Coyne, D. (2020). Potato cyst nematodes: A
 746 new threat to potato production in East Africa. *Front. Plant Sci.* *11*, 670.
 747 10.3389/fpls.2020.00670.
- 748 7. Scholthof, K. B. G., Adkins, S., Czosnek, H., Palukaitis, P., Jacquot, E., Hohn, T., Hohn, B.,
 749 Saunders, K., Candresse, T., Ahlquist, P., Hemenway, C., D. Foster, G. (2011). Top 10 plant
 750 viruses in molecular plant pathology. *Mol. Plant Pathol.* *12*, 938–954. 10.1111/j.1364-
 751 3703.2011.00752.x.
- 752 8. Fangluan, G., Shusuke, K., Ho, S. Y. W., Kazusato, O. (2020). The evolutionary history and global
 753 spatio-temporal dynamics of potato virus Y. *Virus Evol.* *6*, veaa056. 10.1093/ve/veaa056.
- 754 9. Smith, K. M. (1931). Composite nature of certain potato viruses of the mosaic group. *Nature* *127*,
 755 702–702. 10.1038/127702a0.
- 756 10. Wu, X. Y., Ji, Z. S. (2021). An overview on plant viral diseases and antiviral agents. *World Pestic.*

- 757 43, 17–24. 10.16201/j.cnki.cn10-1660/tq.2021.05.03.
- 758 11. Zhang, J., He, F. C., Chen, J. X., Wang, Y. J., Yang, Y. Y., Hu, D. Y., Song, B. A. (2021). Purine
759 nucleoside derivatives containing a sulfa ethylamine moiety: Design, synthesis, antiviral
760 activity, and mechanism. *J. Agric. Food Chem.* *69*, 5575–5582. 10.1021/acs.jafc.0c06612.
- 761 12. Zhang, J., Zhao, L., Zhu, C., Wu, Z. X., Zhang, G. P., Gan, X. H., Liu, D. Y., Pan, J., Hu, D. Y.,
762 Song, B. A. (2017). Facile synthesis of novel vanillin derivatives incorporating a bis (2-
763 Hydroxyethyl) dithioacetal moiety as antiviral agents. *J. Agric. Food Chem.* *65*, 4582–4588.
764 10.1021/acs.jafc.7b01035.
- 765 13. Kežar, A., Kavčič, L., Polák, M., Nováček, J., Gutiérrez-Aguirre, Ion., Žnidarič, M. T., Coll, A.,
766 Stare, K., Gruden, K., Ravnikar, M., Pahovnik, D., Žagar, E., Merzel, F., Anderluh, G.,
767 Podobnik, M. (2019). Structural basis for the multitasking nature of the potato virus Y coat
768 protein. *Sci. Adv.* *5*, eaaw3808. 10.1126/sciadv.aaw3808.
- 769 14. Wu, Z., Ma, G., Zhu, H., Chen, M., Huang, M., Xie, X., Li, X.Y. (2022). Plant viral coat proteins
770 as biochemical targets for antiviral compounds. *J. Agric. Food Chem.* *70*, 8892–8900.
771 10.1021/acs.jafc.2c02888.
- 772 15. Wei, C. L., Zhao, C. N., Li, J., Li, C. Y., Song, B. A., Song, R. J. (2024). Innovative
773 arylimidazole-fused phytovirucides via carbene-catalyzed [3+4] cycloaddition: Locking viral
774 cell-to-cell movement by out-competing virus capsid-host interactions. *Adv. Sci.* 2309343.
775 10.1002/advs.202309343.
- 776 16. Yang, Y. Y., Song, R. J., Yin, L. M., Han, K. L., Yan, F., Song, B.A. (2023). Inactivating activities
777 and mechanism of imidazo[1, 2-*c*]pyrimidin 5(6*H*)-one nucleoside derivatives incorporating a
778 sulfonamide scaffold. *J. Agric. Food Chem.* *71*, 7977–7987. 10.1021/acs.jafc.2c08129.
- 779 17. Zan, N. N., Li, J., He, H. F., Hu, D. Y., Song, B. A. (2021). Discovery of novel chromone
780 derivatives as potential anti-TSWV agents. *J. Agric. Food Chem.* *69*, 10819–10829.
781 10.1021/acs.jafc.1c03626.
- 782 18. Xie, D. D., Zhang, J., Yang, H. Y., Liu, Y. W., Hu, D. Y., Song, B. A. (2019). First anti-ToCV
783 activity evaluation of glucopyranoside derivatives containing a dithioacetal moiety through a
784 novel ToCV CP-oriented screening method. *J. Agric. Food Chem.* *67*, 7243–7248.
785 10.1021/acs.jafc.9b01265.
- 786 19. Wienken, C. J., Baaske, P., Rothbauer, U., Braun, D., Duhr, S. (2010). Protein-binding assays in
787 biological liquids using microscale thermophoresis. *Nat. Commun.* *1*, 100.
788 10.1038/ncomms1093.
- 789 20. Mishra, S., Malhotra, N., Laleu, B., Chakraborti, S., Yogavel, M., Sharma, A. (2024). ATP
790 mimetics targeting prolyl-tRNA synthetases as a new avenue for antimalarial drug
791 development. *iScience.* 10.1016/j.isci.2024.110049.
- 792 21. Kashman, Y., Gustafson, K. R., Fuller, R. W., Cardellina, J. H. I., McMahon, J. B., Currens, M.J.,
793 Buckheit, R. W. J., Hughes, S. H., Cragg, G. M., Boyd, M. R. (1992). The calanolides, a novel
794 HIV-inhibitory class of coumarin derivatives from the tropical rainforest tree *Calophyllum*
795 *lanigerum*. *J. Med. Chem.* *35*, 2735–2743. 10.1021/jm00093a004.
- 796 22. Dai, J. M., Mi, Q. L., Li, X. M., Gang, D., Yang, G. Y., Zhang, J. D., Wang, J., Li, Y. K., Yang,
797 H. Y., Miao, D., Li, Z. J., Hu, Q. F. (2023). The anti-TMV potency of the tobacco-derived
798 fungus *Aspergillus versicolor* and its active alkaloids, as anti-TMV activity inhibitors.
799 *Phytochem.* *205*, 113485. 10.1016/j.phytochem.2022.113485.
- 800 23. He, F. C., Shi, J., Wang, Y. J., Wang, S. B., Chen, J. X., Gan, X. H., Song, B. A., Hu, D. Y. (2019).

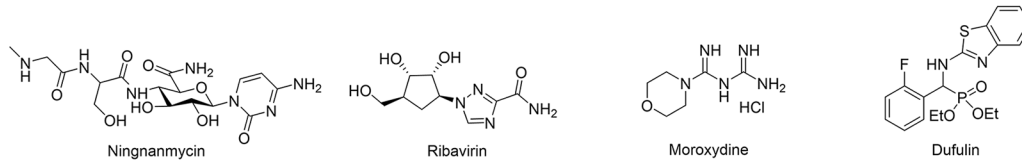
- 801 Synthesis, antiviral activity, and mechanisms of purine nucleoside derivatives containing a
802 sulfonamide moiety. *J. Agric. Food Chem.* *67*, 8459–8467. 10.1021/acs.jafc.9b02681.
- 803 24. Wei, C. L., Yang, X., Shi, S. J., Bai, L., Hu D. Y., Song, R. J., Song, B. A. (2023). 3-Hydroxy-
804 2-oxindole derivatives containing sulfonamide motif: Synthesis, antiviral activity, and modes
805 of action. *J. Agric. Food Chem.* *71*, 267–275. 10.1021/acs.jafc.2c06881.
- 806 25. Zhao, L., Hu, D. Y., Wu, Z. X., Wei, C. L., Wu, S., Song, B. A. (2022). Coumarin derivatives
807 containing sulfonamide and dithioacetal moieties: Design, synthesis, antiviral activity, and
808 mechanism. *J. Agric. Food Chem.* *70*, 5773–5783. 10.1021/acs.jafc.2c00672.
- 809 26. Li, C. Y., Song, R. J., He, S. Q., Wu, S. K., Wu, S., Wu, Z. X., Hu, D. Y., Song, B. A. (2022).
810 First discovery of imidazo[1,2-*a*]pyridine mesoionic compounds incorporating a sulfonamide
811 moiety as antiviral agents. *J. Agric. Food Chem.* *70*, 7375–7386. 10.1021/acs.jafc.2c01813.
- 812 27. Bektas, Y., Rodriguez-Salus, M., Schroeder, M., Gomez, A., Kaloshian, I., Eulgem, T. (2016).
813 The synthetic elicitor DPMP (2, 4-dichloro-6-*{(E)-[(3-methoxyphenyl) imino] methyl}* phenol)
814 triggers strong immunity in *Arabidopsis thaliana* and tomato. *Sci Rep-UK* *6*, 29554.
815 10.1038/srep29554.
- 816 28. Kumar, K. S., Ganguly, S., Veerasamy, R., De Clercq, E. (2010). Synthesis, antiviral activity and
817 cytotoxicity evaluation of Schiff bases of some 2-phenyl quinazoline-4 (3) *H*-ones. *Eur. J Med.*
818 *Chem.* *45*, 5474–5479. 10.1016/j.ejmech.2010.07.058.
- 819 29. Ramadan, W. S., Saber-Ayad, M. M., Saleh, E., Abdu-Allah, H. H., Abdel-nasser, A., Menon,
820 V., El-Shorbagi, A. A., Menon, V., Tarazi, H., Semreen, M. H., Soares, N. C., Hafezi, H.,
821 Venkatakhalaam, T., Ahmed, S., Kanie, O., Hamoudi, R., El-Awady, R. (2024). Design,
822 synthesis and mechanistic anticancer activity of new acetylated 5-aminosalicylate-thiazolinone
823 hybrid derivatives. *iScience* *27*, 108659. 10.1016/j.isci.2023.108659.
- 824 30. Zhang, H., Tian, Y., Kang, D. W., Huo, Z. P., Zhou, Z. X., Liu, H. Q., Clercq, E. D., Pannecouque,
825 C., Zhan, P., Liu X. Y. (2017). Discovery of uracil-bearing DAPYs derivatives as novel HIV-1
826 NNRTIs via crystallographic overlay-based molecular hybridization. *Eur. J Med. Chem.* *130*,
827 209–222. 10.1016/j.ejmech.2017.02.047.
- 828 31. Ravichandran, V., Kumar, B. P., Sankar, S., Agrawal, R. K. (2009). Predicting anti-HIV activity
829 of 1, 3, 4-thiazolidinone derivatives: 3D-QSAR approach. *Eur. J Med. Chem.* *44*, 1180-1187.
830 10.1016/j.ejmech.2008.05.036.
- 831 32. Bai, L., Wei, C. L., Shen, Z. J., He, H. F., Yang, X., Shi, S. J., Hu, D. Y., Song, B. A. (2023).
832 Splicing indoles and 4,5-dihydro-1*H*-pyrazoline structure gave birth to novel antiviral agents:
833 Design, synthesis, and mechanism study. *J. Agric. Food Chem.* *71*, 7239–7249.
834 10.1021/acs.jafc.3c01005.
- 835 33. Marzaro, G., Guiotto, A., Borgatti, M., Finotti, A., Gambari, R., Breveglieri, G., Chilin, A.
836 (2013). Psoralen derivatives as inhibitors of NF- κ B/DNA interaction: synthesis, molecular
837 modeling, 3D-QSAR, and biological evaluation. *J Med. Chem.* *56* 1830–1842.
838 10.1021/jm3009647.
- 839 34. Sun, Z. R., Wei, C. L., Wu, S., Zhang, W. B., Song, R. J., Hu, D. Y. (2022). Synthesis, anti-potato
840 virus Y activities, and interaction mechanisms of novel quinoxaline derivatives bearing
841 dithioacetal moiety. *J. Agric. Food Chem.* *70*, 7029–7038. 10.1021/acs.jafc.2c01898.
- 842 35. Li, J., Zan, N. N., He, H. F., Hu, D. Y., Song, B. A. (2023). Piperazine Derivatives containing
843 the α -ketoamide moiety discovered as potential anti-tomato spotted wilt virus agents. *J. Agric.*
844 *Food Chem.* *71*, 6301–6313. 10.1021/acs.jafc.3c01361.

- 845 36. Zamora, M., Méndez-López, E., Agirrezabala, X., Cuesta, R., Lavín, J. L., Sánchez-Pina, M. A.,
846 Aranda, M. A., Valle, M. (2017). Potyvirus virion structure shows conserved protein fold and
847 RNA binding site in ssRNA viruses. *Sci. Adv.* *3*, eaao2182. 10.1126/sciadv.aao2182.
- 848 37. Agirrezabala, X., Mendez-Lopez, E., Lasso, G., Sánchez-Pina, M. A., Aranda, M., Valle, M.
849 (2015). The near-atomic cryoEM structure of a flexible filamentous plant virus shows
850 homology of its coat protein with nucleoproteins of animal viruses. *eLife* *4*, e11795.
851 10.7554/elife.11795.
- 852 38. Jagadish, M. N., Huang, D., Ward, C. W. (1993). Site-directed mutagenesis of a potyvirus coat
853 protein and its assembly in *Escherichia coli*. *J. Gen. Virol.* *74*, 893–896. 10.1099/0022-1317-
854 74-5-893.
- 855 39. Dolja, V. V., Haldeman-Cahill, R., Montgomery, A. E., Vandenbosch, K. A., Carrington, J. C.
856 (1995). Capsid protein determinants involved in cell-to-cell and long distance movement of
857 tobacco etch potyvirus. *Virology* *206*, 1007–1016. 10.1006/viro.1995.1023.
- 858 40. Yan, Z. Y., Xu, X. J., Fang, L., Geng, C., Tian, Y. P., Li, X. D. (2021). Multiple aromatic amino
859 acids are involved in potyvirus movement by forming π -stackings to maintain coat protein
860 accumulation. *Phytopathol. Res.* *3*, 10. 10.1186/s42483-021-00088-9.
- 861 41. Yan, Z. Y., Xu, X. J., Fang, L., Cheng, D. J., Tian, Y. P., Geng, C., Li, X. D., Valkonen, J. P.
862 (2021). Residues R192 and K225 in RNA-binding pocket of tobacco vein banding mosaic virus
863 CP control virus cell-to-cell movement and replication. *Mol. Plant Microbe In.* *34*, 658–668.
864 10.1094/mpmi-09-20-0265-r.
- 865 42. Wang, A. (2021). Cell-to-cell movement of plant viruses via plasmodesmata: a current
866 perspective on potyviruses. *Curr. Opin. Virol.* *48*, 10–16. 10.1016/j.coviro.2021.03.002.
- 867 43. Zhao, R. Y., Fu, L. L., Yuan, Z. X., Liu, Y., Zhang, K., Chen, Y. M., Wang, L. M., Sun, D. J.,
868 Chen, L.X., Liu, B., Zhang, L. (2021). Discovery of a novel small-molecule inhibitor of
869 Fam20C that induces apoptosis and inhibits migration in triple negative breast cancer. *Eur. J.*
870 *Med. Chem.* *210*, 113088. 10.1016/j.ejmech.2020.113088.
- 871 44. An, H., Lee, S., Lee, J. M., Jo, D. H., Kim, J., Jeong, Y. S., Heo, M. J., Cho, C. S., Choi, H., Seo,
872 J. H., Hwang, S., Lim, J., Kim, T., Jun, H. O., Sim, J., Lim, C., Hur, J., Ahn, J., Kim, H. S.,
873 Seo, S. Y., Na, Y., Kim, S. H., Lee, J., Lee, J., Chung, S. J., Kim, Y. M., Kim, K. W., Kim, S.
874 G., Kim, J. H., Suh, Y. G. (2018). Novel hypoxia-inducible Factor 1 α (HIF-1 α) inhibitors for
875 angiogenesis-related ocular diseases: Discovery of a novel scaffold via ring-truncation strategy.
876 *J. Med. Chem.* *61*, 9266–9286. 10.1021/acs.jmedchem.8b00971.
- 877 45. Iannelli, D., D'Apice, L., Cottone, C., Viscardi, M., Scala, F., Zoina, A., Del Sorbo, G., Spigno,
878 P., Capparelli, R. (1997). Simultaneous detection of cucumber mosaic virus, tomato mosaic
879 virus and potato virus Y by flow cytometry. *J. Virol. Methods.* *69*, 137–145. 10.1016/s0166-
880 0934(97)00149-3.
- 881 46. Cheng, D. J., Tian, Y. P., Geng, C., Guo, Y., Jia, M. A., Li, X. D. (2020). Development and
882 application of a full-length infectious clone of potato virus Y isolate belonging to SYR-I strain.
883 *Virus Res.* *276*, 197827. 10.1016/j.virusres.2019.197827.
- 884 47. Liu, H., Naismith, J. H. (2008). An efficient one-step site-directed deletion, insertion, single and
885 multiple-site plasmid mutagenesis protocol. *BMC Biotechnol.* *8*, 1–10. 10.1186/1472-6750-8-
886 91.
- 887 48. Hellinen, L., Bahrpeyma, S., Rimpelä, A. K., Hagström, M., Reinisalo, M., Urtti, A. (2020)
888 Microscale thermophoresis as a screening tool to predict melanin binding of drugs. *Pharmaceutics.*

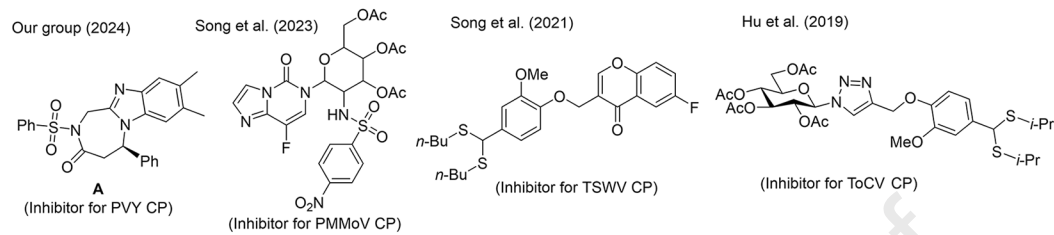
889 12, 554. 10.3390/pharmaceutics12060554.

Journal Pre-proof

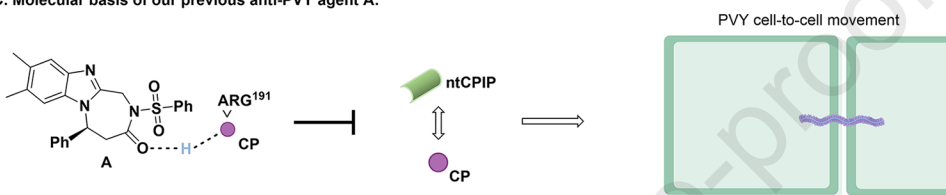
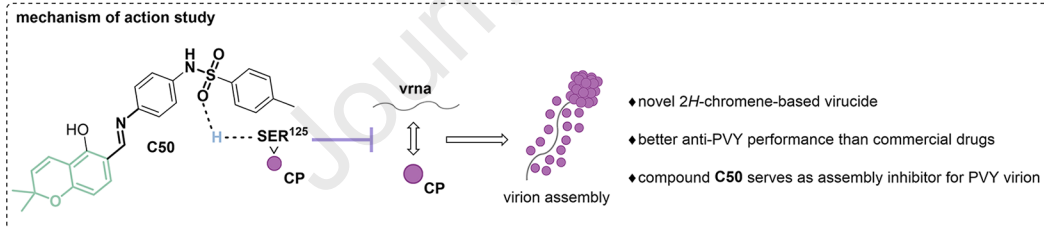
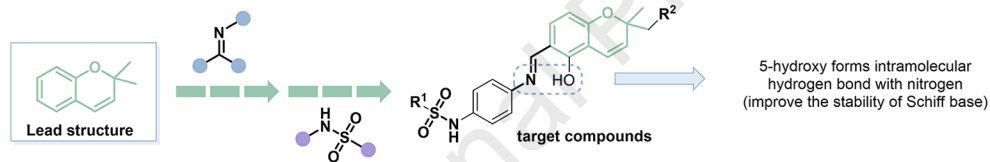
A. Active ingredients in common commercial antiviral agents for plants:

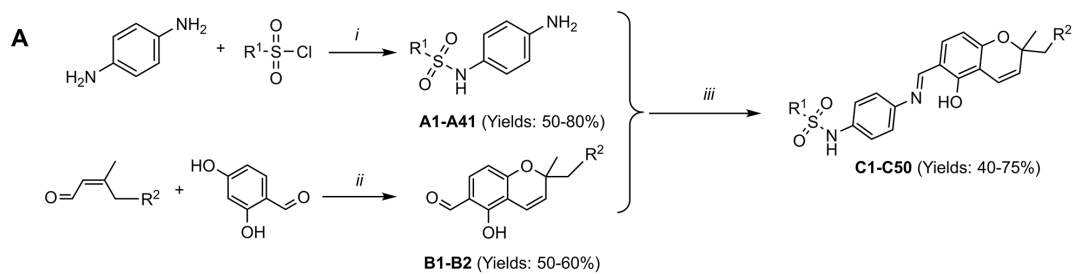


B. Some reported phytoviral CP inhibitors:

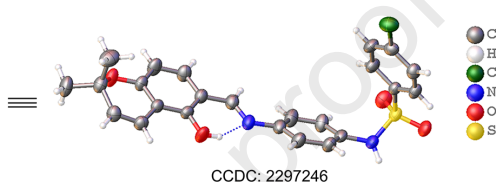
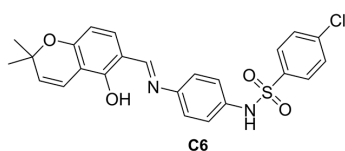


C. Molecular basis of our previous anti-PVY agent A:

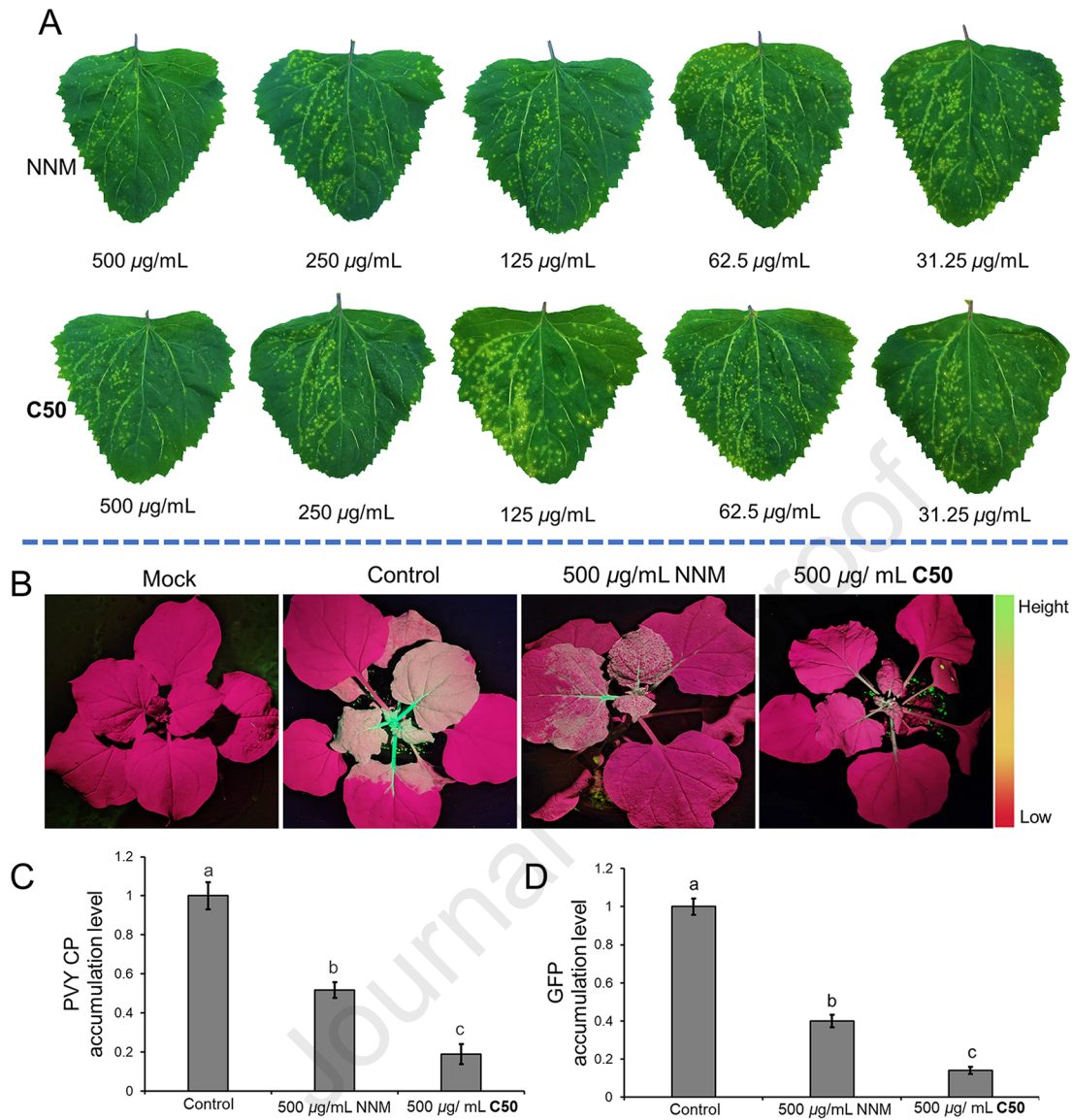
D. *This work*: 2,2-dimethyl-2H-chromene-based lead optimization incorporating sulfonamides and Schiff bases

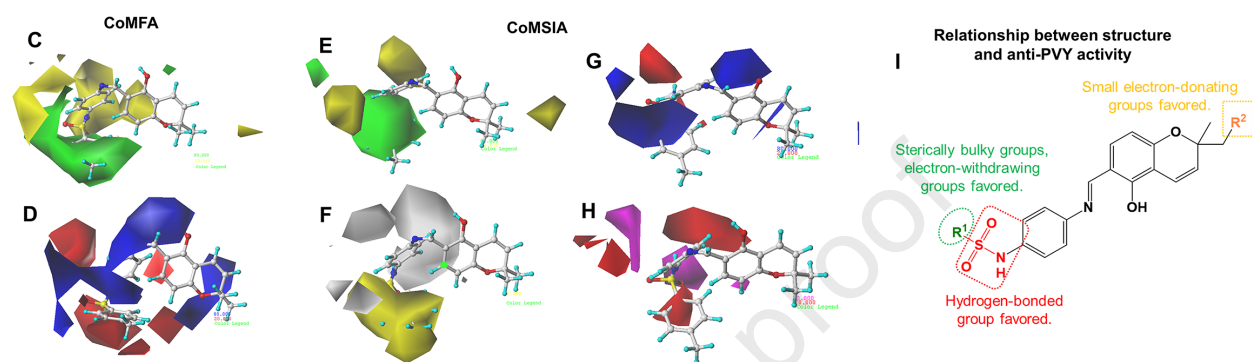
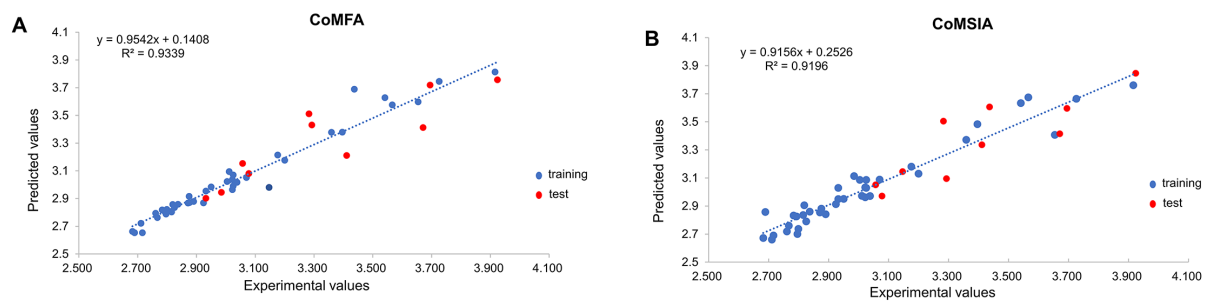


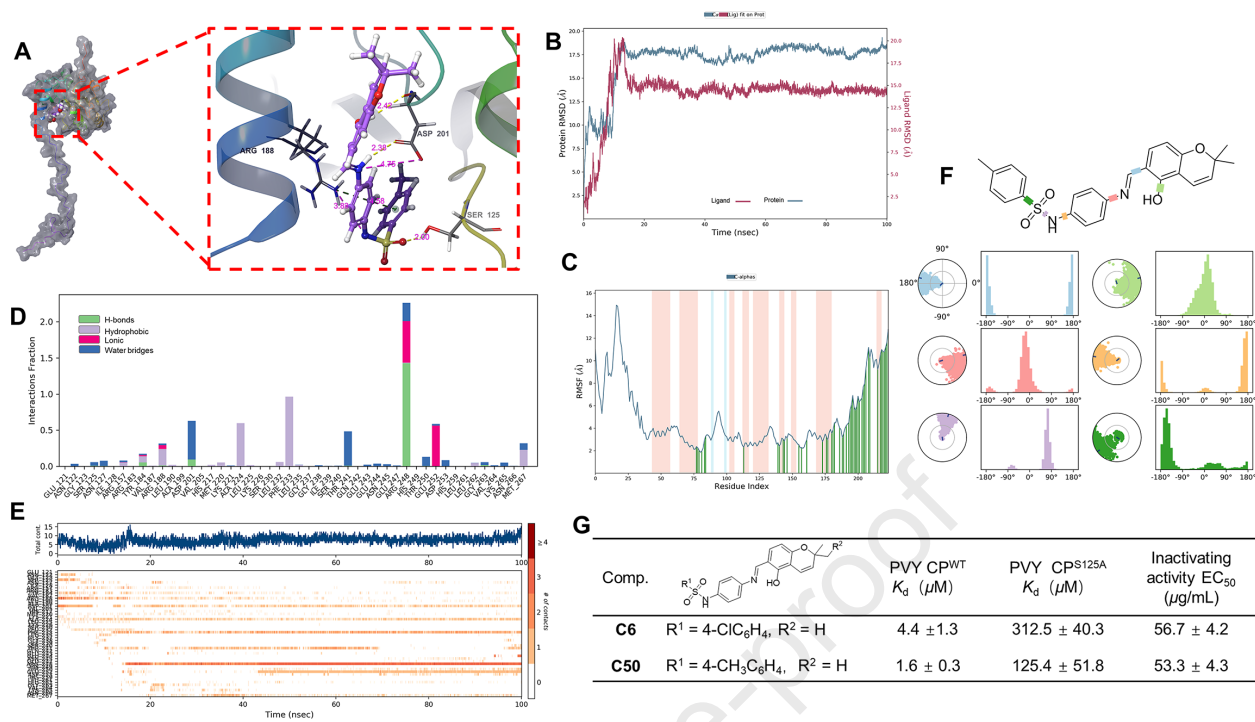
- | | | | | |
|---|--|--|---|--|
| C1 R ¹ = 4-OCH ₃ C ₆ H ₄ , R ₂ =H | C11 R ¹ =3-CNC ₆ H ₄ , R ² =H | C21 R ¹ =4-CH ₃ CONHC ₆ H ₄ , R ² =H | C31 R ¹ =2,4-di-ClC ₆ H ₃ , R ² =H | C41 R ¹ =4-ClC ₆ H ₄ , R ² = |
| C2 R ¹ =4-CF ₃ C ₆ H ₄ , R ₂ =H | C12 R ¹ =4-NO ₂ C ₆ H ₄ , R ² =H | C22 R ¹ =2-CF ₃ C ₆ H ₄ , R ² =H | C32 R ¹ =2,6-di-FC ₆ H ₃ , R ² =H | C42 R ¹ =4-CH ₃ C ₆ H ₄ , R ² = |
| C3 R ¹ =(CH ₂) ₇ CH ₃ , R ₂ =H | C13 R ¹ =Cyclopropane, R ² =H | C23 R ¹ =3,5-di-ClC ₆ H ₃ , R ² =H | C33 R ¹ =2-BrC ₆ H ₄ , R ² =H | C43 R ¹ =5-Cl-Thiophen-2-yl, R ² = |
| C4 R ¹ =Thiophene-2-yl, R ₂ =H | C14 R ¹ =2,5-di-ClC ₆ H ₃ , R ² =H | C24 R ¹ =5-Cl-Thiophene-2-yl, R ² =H | C34 R ¹ =4-BrC ₆ H ₄ , R ² =H | C44 R ¹ =3-CH ₃ C ₆ H ₄ , R ² = |
| C5 R ¹ =4-FC ₆ H ₄ , R ₂ =H | C15 R ¹ =2,5-di-FC ₆ H ₃ , R ² =H | C25 R ¹ =2-ClC ₆ H ₄ , R ² =H | C35 R ¹ =3-CF ₃ C ₆ H ₄ , R ² =H | C45 R ¹ =3-FC ₆ H ₄ , R ² = |
| C6 R ¹ =4-ClC ₆ H ₄ , R ₂ =H | C16 R ¹ =3-BrC ₆ H ₄ , R ² =H | C26 R ¹ =3,5-di-FC ₆ H ₃ , R ² =H | C36 R ¹ =3-ClC ₆ H ₄ , R ² =H | C46 R ¹ =4-CF ₃ C ₆ H ₄ , R ² = |
| C7 R ¹ =3-FC ₆ H ₄ , R ₂ =H | C17 R ¹ =C ₆ H ₅ , R ² =H | C27 R ¹ =3-CH ₃ C ₆ H ₄ , R ² =H | C37 R ¹ =2-F-3-ClC ₆ H ₃ , R ² =H | C47 R ¹ =2,6-di-FC ₆ H ₃ , R ² = |
| C8 R ¹ =2-FC ₆ H ₄ , R ₂ =H | C18 R ¹ =4-CH ₃ CH ₂ C ₆ H ₄ , R ² =H | C28 R ¹ =Benzyl, R ² =H | C38 R ¹ =2-CH ₃ -3-ClC ₆ H ₃ , R ² =H | C48 R ¹ =3,5-di-FC ₆ H ₃ , R ² = |
| C9 R ¹ = Pyridin-3-yl, R ₂ =H | C19 R ¹ =2,4,6-tri-CH ₃ C ₆ H ₂ , R ² =H | C29 R ¹ =(CH ₂) ₃ CH ₃ , R ² =H | C39 R ¹ =2,5-di-CH ₃ -Isoxazol-4-yl, R ² =H | C49 R ¹ =5-Br-Thiophen-2-yl, R ² = |
| C10 R ¹ =5-Br-Thiophene-2-yl, R ₂ =H | C20 R ¹ =4- <i>tert</i> -butyl-C ₆ H ₄ , R ² =H | C30 R ¹ =4-OCF ₃ C ₆ H ₄ , R ² =H | C40 R ¹ =L(-)-10-Camphoryl, R ² =H | C50 R ¹ =4-CH ₃ C ₆ H ₄ , R ² =H |

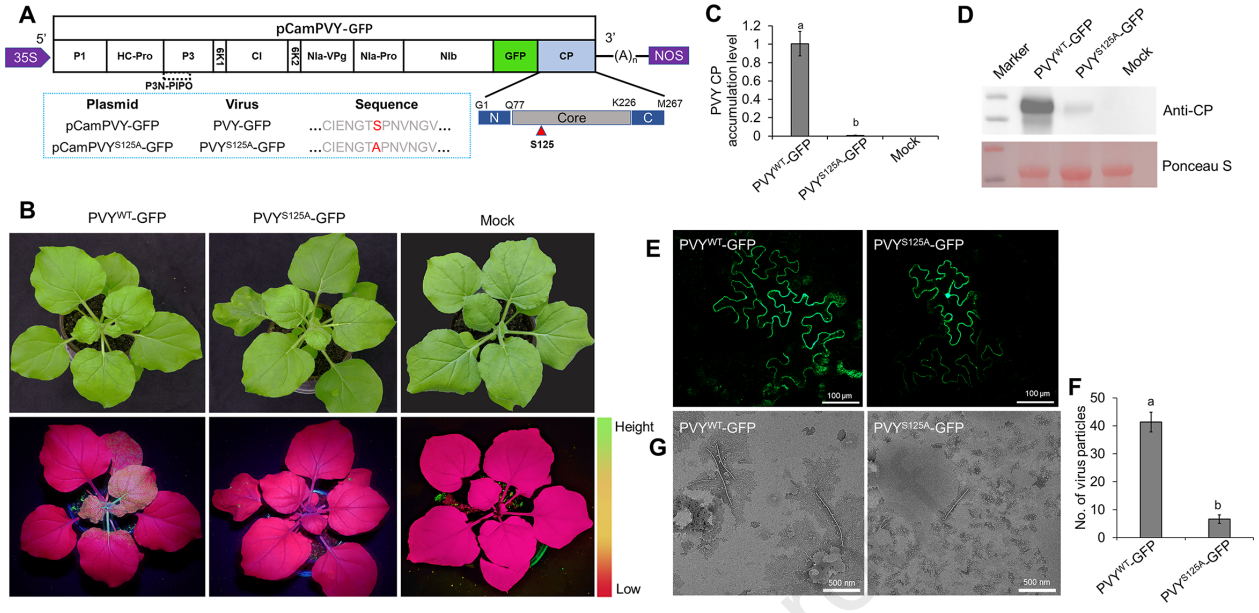
B

Journal Pre-proof

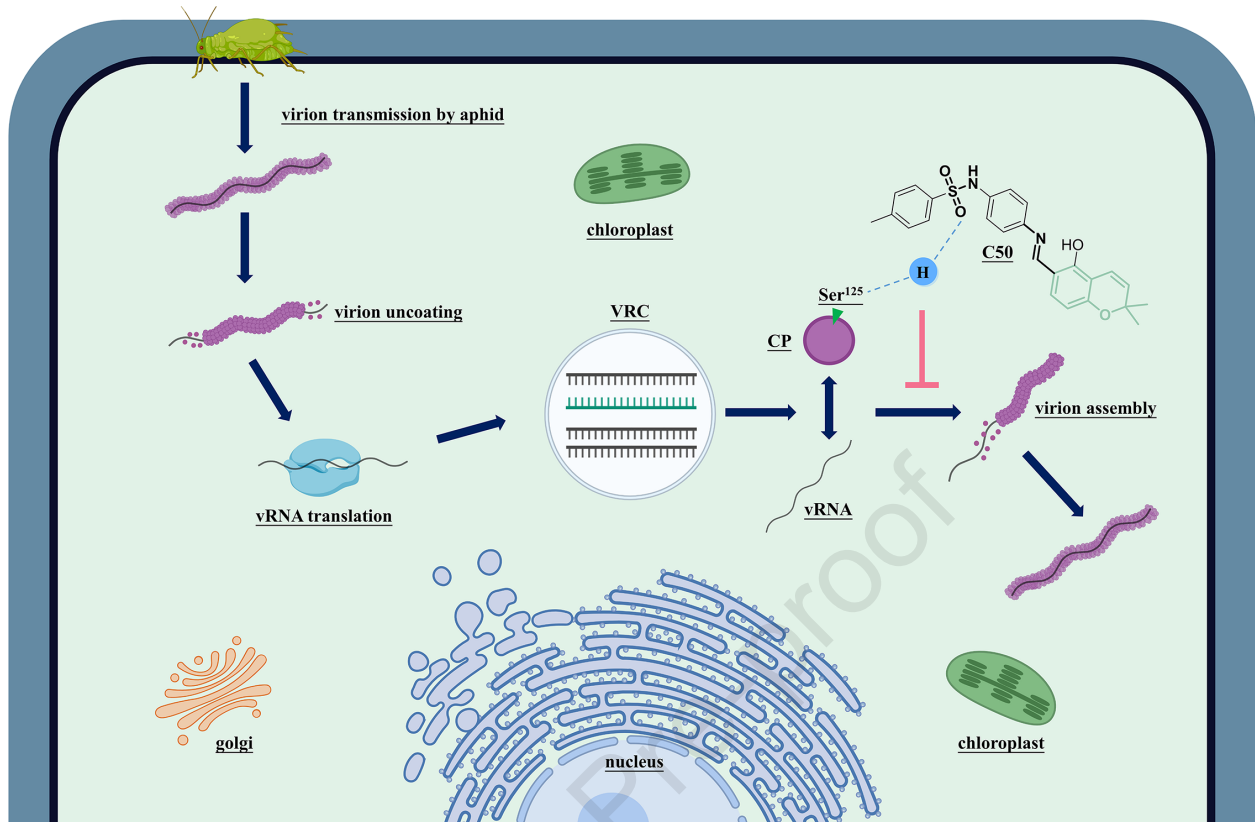








Journal Pre-proof



Highlights

1. Discovery of 2H-chromene derivatives with potent inhibitory activity against PVY.
2. Constructed 3D-QASR models of 2H-chromene derivatives to guide compound optimization.
3. Discovery of inhibitors for PVY particle assembly based on the PVY CP conserved region.
4. Point mutation strategy to validate the effect of potential sites on PVY function.

Journal Pre-proof

KEY RESOURCES TABLE

REAGENT or RESOURCE	SOURCE	IDENTIFIER
Antibodies		
anti-GFP	Proteintech	Cat#66002-1-Ig
anti- PVY CP	Youke	Custom synthesis, http://www.youke-ab.cn/
Horseradish peroxidase-conjugated goat anti-rabbit IgG	Proteintech	Cat#SA00001-2
Bacterial and virus strains		
<i>Escherichia coli</i> DH5 α Competent Cells	Sangon Biotech	Cat#B528413-0010
<i>Escherichia coli</i> BL21 (DE3) Competent Cells	Sangon Biotech	Cat#B528414-0010
Agrobacterium GV3101 Competent Cells	Sangon Biotech	Cat#B528430-0010
Potato virus Y	Our laboratory collection	N/A
Biological samples		
<i>Nicotiana benthamiana</i>	Our laboratory collection	N/A
<i>Nicotiana tabacum</i> K326	Our laboratory collection	N/A
<i>Chenopodium amaranticolor</i>	Our laboratory collection	N/A
Chemicals, peptides, and recombinant proteins		
Isopropyl β -D-1-thiogalactopyranoside	Sangon Biotech	Cat#A600168-0005
2,4-dihydroxybenzaldehyde	Energy Chemical	Cas: 95-01-2
3-methylbut-2-enal	Energy Chemical	Cas: 107-86-8
citral	Energy Chemical	Cas: 5392-40-5
<i>p</i> -phenylenediamine	Energy Chemical	Cas: 106-50-3
Substituted sulfonyl chloride	Energy Chemical	N/A
DMSO- d_6	Energy Chemical	Cas: 2206-27-1
Ningnanmycin	Bide Pharmatech	Cas: 156410-09-2
Ponceau S	Sangon Biotech	Cat#A610437-0025
PVY CP	Wei <i>et al.</i> (2024) ¹⁵	DOI:10.1002/adv.202309343
PVY CP ^{S125A}	This paper	N/A
Critical commercial assays		
Trizol reagent	Invitrogen	Cat#15596026
HiScript III 1st Strand cDNA Synthesis Kit (+gDNA wiper)	Vazyme	Cat#R312-01
TB Green	TaKaRa	Cat#R820A
Monolith RED-NHS second generation protein labeling kit	NanoTemper	Cat#MO-L011
Deposited data		
Potato Virus Y coat protein structure	Kežar <i>et al.</i> (2019) ¹³	PDB (entry 6HXX)
(<i>E</i>)-4-chloro- <i>N</i> -(4-(((5-hydroxy-2,2-dimethyl-2 <i>H</i> -chromen-6-yl)methylene)amino)phenyl) benzenesulfonamide crystallographic data	This paper	CCDC No. 2297246
Oligonucleotides		
Primers used for DNA amplification, RT-qPCR and mutagenesis	This paper	See Supplementary information (Table S2)
Recombinant DNA		
pCAMBIA0390 expression vector for PVY-GFP	Cheng <i>et al.</i> (2020) ⁴⁶	DOI:10.1016/j.virusres.2019.197827
pCAMBIA0390 expression vector for PVY ^{S125A} -GFP	This paper	N/A

pET32a (+) expression vector for PVY CP	Sangon Biotech	Custom synthesis, https://www.sangon.com
pET32a (+) expression vector for PVY CP ^{S125A}	Sangon Biotech	Custom synthesis, https://www.sangon.com
Software and algorithms		
NanoTemper Monolith Instrument (NT.115) Control and Analysis Software Package	NanoTemper	https://nanotempertech.com/microscale-thermophoresis
SYBYL-2.1	Tripos	https://www.tripos.com
Schrödinger Maestro 13.5	Schrödinger	https://www.schrodinger.com
MestReNova	Mestrelab Research	https://www.mestrelab.cn.com
SPSS 26.0	IBM	https://www.ibm.com
Microsoft Excel 2021	Microsoft	https://www.microsoft.com
ZEN 2.1	ZEISS	https://www.zeiss.com
ChemDraw 23	CambridgeSoft	https://www.chemdraw.com.cn
Chemi Doc MP Imaging System	Bio-Rad	https://www.bio-rad.com
Desmond	Schrödinger	https://www.schrodinger.com
Other		
Copper mesh carbon support film	Zhongjingkeyi	Cat#BZ11022a